JULY, 2013

Analysis of chemical bonding by means of reduced density matrices

Roberto Álvarez Boto

Master Thesis

European Master in
Theoretical Chemistry and Computational Modelling

JULIO, 2013

Análisis del enlace químico mediante matrices densidad reducidas

Roberto Álvarez Boto

Tésis de Máster

Máster europeo en
Química Teórica y Modelización Computacional

D. Ángel Martín Pendás, Catedrático del Departamento de Química Física y Analítica de la Universidad de Oviedo y Coordinador del Máster Europeo en Química Teórica y Modelización Computacional,

CERTIFICA:

Que el trabajo titulado **Análisis del enlace químico mediante matrices densidad reducidas** ha sido realizado por Roberto Álvarez Boto, bajo la tutela del catedrático D. Ángel Martín Pendás con el fin de optar al título que otorga el Máster Europeo en Química Teórica y Modelización Computacional.

Oviedo, 15 de julio de 2013

Fdo.: Ángel Martín Pendás
Coordinador del Máster Europeo en Química Teórica y Modelización Computacional

D. Ángel Martín Pendás, Catedrático de Química Física del Departamento de Química Física y Analítica de la Universidad de Oviedo,

CERTIFICA:

Que el trabajo titulado **Análisis del enlace químico mediante matrices densidad reducidas**, ha sido realizado bajo su dirección por Roberto Álvarez Boto, constituyendo su Tésis de Máster, cuya presentación autoriza.

Oviedo, 15 de julio de 2013

Fdo.: Ángel Martín Pendás

Agradecimientos

Son muchos a los que debo agradecer que haya podido completar este trabajo. Espero no olvidarme de nadie.

A mis compañeros de laboratorio. Alfonso, Mamel, Miriam, David y Marcos por nuestras absurdas y divertidas conversaciones y hacer del laboratorio mi segunda casa. No me quiero olvidar del pinche Marco ni de Alberto y sus instructivas discusiones sobre el uso del castellano.

A mis compañeros de máster, por los buenos momentos vividos en Oviedo, Zaragoza y Perugia. El M1 sería interminable sin vuestra compañía.

A Ángel, Evelio, Aurora, Victor y Michi por su apoyo y dedicación. Especialmente a Ángel y Evelio, por su paciencia, y por enseñarme a pensar con cierto sentido crítico.

A Julia, Mónica y Marcos de nuevo, por ser mis embajadores personales en París. A Christophe y Sehr por sufir mi terrible francés. Nunca esperé recibir tanto de una estancia tan corta.

Finalmente quisiera dar las gracias a todo aquel que se aventure a leer este trabajo.

Gracias a todos.

A mi familia.

Abstract

The modern Theory of Chemical Bonding may be well understood as the study of reduced density matrices (RDMs) in real space regions to get new insights of the chemical bond. Although, much work has been widely used to understand chemical bonding from one-electron density, include correlation effects requires the access to higher order densities. Based on the cumulant expansion of the RDMs, a set of bonding indices which may decomposed into one-electron component may be defined. Each component is partnered with a one-electron function(natural adaptive orbital, NAdO). Additionally to correlation effects, the renewed interest on long-range interactions, has moved chemists to developed new tools for understanding these interaction. NCI analysis has been arose as one of the most accepted index for exploring noncovalent interactions. Recently, it was shown that ionic interactions may be grasp by NCI index, but not much work has been carried out to understand the behavior of NCI in covalent bonds. In the present work, a comparative NAdOs and NCI analysis of the a set of small molecules has been carried out. As example of long range interaction, we examined the validity of the NCI index to analysis the bonding in a self assembly monolayer (SAM) of octylamine.

Contents

1 Methods of Quantum Mechanics **17**
- 1.1 The Hartree-Fock aproximation . . . 18
- 1.2 Configurations Interaction . . . 19
  - 1.2.1 CI matrix . . . 20
  - 1.2.2 Correlation energy . . . 21
- 1.3 Multiconfigurational Methods . . . 21
- 1.4 Density Functional Theory . . . 22
  - 1.4.1 First Hohenberg-Kohn theorem . . . 22
  - 1.4.2 Second Hohenberg-Kohn theorem . . . 23
- 1.5 Density matrices and Related Functions . . . 25
  - 1.5.1 The Electron Distribution . . . 25
- 1.6 Reduced Density Matrices . . . 26
  - 1.6.1 Cumulants from n-RDMs . . . 27
  - 1.6.2 nCDMs at single determinant level . . . 28
  - 1.6.3 Pair density and electron correlation . . . 29

2 Topology **31**
- 2.1 The Gradient Vector Field . . . 31
- 2.2 Topology of the charge density . . . 33
- 2.3 Quantum Theory of Atoms in Molecule . . . 34
  - 2.3.1 Atomic Properties . . . 34

3 Chemical bonding in real space **39**
- 3.1 Pair density and electron localization . . . 39
- 3.2 Generalized population analysis . . . 41
- 3.3 Reduced Density Gradient . . . 45
  - 3.3.1 Shell structure as described by s . . . 45
  - 3.3.2 Revealing NonCovalent Interactions . . . 47

4 Results **51**
- 4.1 Examples and Computational Details . . . 51
  - 4.1.1 Illustrative Results . . . 51

5 Conclusiones **67**

6 Appendix **69**

Introduction

Many of our chemical and physical understanding of the structure and properties of the matter are based on the idea that their elemental parts remain invariant. The predictive character of matter science, is a consequence of the invariance and the transferability of the properties of atoms and ions forming the matter. Turning to quantum mechanics, the system is treated as a whole, being not possible to recover the basic chemical concepts.

Valence Bond and Molecular Orbital theories were the first attempts to overcome this hitch. Many of the concepts introduced in these old days, such as atomic charges, covalency, ionicity, resonance,etc have been firmly rooted in the chemistry parlance. Although both theories were widely accepted (at the beginning the MO theory was more fortunate than VB), it was found that many of the concepts defined by them, are highly dependent on the accuracy of the wave function.

John Coleman [1] in the 60's claimed to replace wave function role by reduce density matrices (RDMs), but were the formulation of the Density Functional Theory (DFT) by Hohenberg and Kohn [2] and the development of Quantum Theory of Atoms in Molecules (QTAIM) by R.F.W. Bader [3],the keys to convince the community to leave the wave function analysis based on a orbital space, and focus on the RDMs.

Fixed, RDMs as the key functions, a real space partition is needed to recover chemical concepts. Daudel and co-workers[4] were the first who explore how to split real space. They were looking for the "best" decomposition of physical space into mutually exclusive regions called "lodges". The partition proposed by Daudel and the subsequently work of Bader and co-workers set the basis of what Paul L. A. Popelier has defined as the Quantum Chemical Topology (QCT)[5]. The topological approaches encompass all the real space partitions based on the topology of any chemically meaningful scalar function, constructed from the RDM. It thus provides provides quantities that are invariant under orbital transformations. These last property, makes any index defined in the QCT almost independent of the theoretical framework use to obtain the wave function. The electron density, the electron. localization function (ELF)[6], the molecular electrostatic potential (MEP), are some of the most employed functions in QCT to divide the real space. Classical chemical concepts emerge from the topology of any of the above scalar fields. Atom in molecules, appear from the topology the electron density, the electron pairing envisioned by Lewis is recovered by the ELF and ELI-D[7], nucelophilic and electrophilic regions are easily identified by MEP and so on [8].

Applying all this scalar fields to build bonding models, take us to the theory of chemical

bonding. Particularly interesting in this field is the Fermi hole defined by Lennard-Jones [9], many years after used by Bader and Stephens [10] as a measure of the Fermi correlation, and recovered by R. Ponec, defining the domain averaged Fermi hole (DAFH) analysis [11],[12]. The success of DAFH analysis to chemical bonding , convince other authors to generalized Fermi whole analysis. E. Francisco and co-workers generalized the DAFH analysis by means of the RDM, in particular, by their cumulants, recovering bond orders and the one-electron bonding picture from a set of functions knows as Natural Adaptive Orbitals (NAdOs) [13].

Despite the success of the topological approach to tackle with covalent and ionic bonding, identified weak dispersion interactions require some new scalar field. The reduced density gradient has been found to identified successfully strong interactions already found by other fields, ant also the weak dispersion interactions, being the kernel of the so well accepted NCI (non-covalent interactions) method. The properties of $s(\mathbf{r})$ and the curvatures of the the $\rho(\mathbf{r})$, are combined not only to identified any kind of interactions, but to differentiate between them.

In this exploratory work, we performed a deep bonding analysis, covering all kind of interactions. A comparative NAdOs and NCI analysis were performed to the diatomic homonuclear molecules A_2(A=H,He,Li,Be,B,C,N,,O,F,Ne) and the heteronuclear molecules LiH and H_2O. As example of weak dispersive interaction, we choosen to different arrangements of octylamine in gas phase.

The structure of the present work is as follows: in Chapter 1 we reviewed the thoretical methods employed to obtained the wave function. In Chapter 2 we introduced the RDM formalism. Chapter 3 is devoted to the topological approaches and in particular to the QTAIM. In the Chapter 4 we present the NAdOs and the NCI analysis as a tool to analyse chemical bonding. Chapter 5 we apply both methods to the systems aforementioned. We finalize the manuscript gathering a number of conclusions in the Chapter 6.

1 Methods of Quantum Mechanics

Any problem in electronic structure of matter is covered by the Schrödinger equation

$$\mathrm{i}\hbar\frac{\mathrm{d}\Psi}{\mathrm{dt}} = \widehat{\mathrm{H}}\Psi, \tag{1.1}$$

where Ψ is the wave function of the system and $\widehat{\mathrm{H}}$ the hamiltonian operator. For conservative or stationary systems, where the potential energy part of the Hamiltonian is not a function of time, a possible solution of Eq. 1.1 is

$$\Psi = \psi e^{-iEt/\hbar}, \tag{1.2}$$

with

$$\hat{H}\psi = E\psi \tag{1.3}$$

where E is the energy of the system, $\psi = \psi(\mathrm{x}_1, \mathrm{x}_2, ...\mathrm{x}_\mathrm{N})$ is the N-particle time independent wave function, $\mathrm{x_i} = \mathrm{r_i}\sigma_\mathrm{i}$, and r and σ are spatial and spin coordinates, respectively. In atomic units, the Hamiltonian for a molecule formed by N electrons and M nuclei is given by

$$\widehat{\mathrm{H}} = -\frac{1}{2}\sum_{\mathrm{A}=1}^{\mathrm{M}}\nabla_\mathrm{A}^2 - \frac{1}{2}\sum_{\mathrm{i}}^{\mathrm{N}}\nabla_\mathrm{i}^2 + \sum_{\mathrm{i>j}}\frac{1}{\mathrm{r_{ij}}} - \sum_{\mathrm{A,i}}\frac{\mathrm{Z_A}}{|\mathrm{r_i} - \mathrm{R_A}|} + \sum_{\mathrm{A>B}}\frac{\mathrm{Z_A Z_B}}{|\mathrm{R_A} - \mathrm{R_B}|}, \tag{1.4}$$

where the indices $\mathrm{A, B}$ and $\mathrm{i, j}$ designate nuclei and electrons respectively, $\mathrm{Z_A}$ is the nuclear charge of atom A, and ∇_i^2 and ∇_A^2 are the electron and nuclear laplacians, respectively. Under the Born-Oppenheimer approximation the nuclei are considered to have fixed positions, so that the last term is Eq. 1.4 is a constant and the kinetic energy of the nuclei (first term of Eq. 1.4) can be neglected. The remaining terms are called the electronic Hamiltonian.

$$\widehat{\mathrm{H}}_\mathrm{elec} = -\frac{1}{2}\sum_{\mathrm{i}}^{\mathrm{N}}\nabla_\mathrm{i}^2 + \sum_{\mathrm{i>j}}\frac{1}{\mathrm{r_{ij}}} - \sum_{\mathrm{A,i}}\frac{\mathrm{Z_A}}{|\mathrm{r_i} - \mathrm{R_A}|}. \tag{1.5}$$

Similarly to Eq. 1.3, the eigenvalue problem involving $\widehat{\mathrm{H}}_\mathrm{elec}$ is

$$\widehat{\mathrm{H}}_\mathrm{elec}\Psi_\mathrm{elec} = \mathrm{E_{elec}}\Psi_\mathrm{elec}, \tag{1.6}$$

and leads to the electron wave function Ψ_elec and the electron energy $\mathrm{E_{elec}}$. Both depend parametrically on the nuclear positions. The total energy of any arrangement of the nuclei is built by adding the repulsion energy between the nuclei to $\mathrm{E_{elec}}$.

$$\mathrm{E_{total}} = \mathrm{E_{elec}} + \sum_{\mathrm{A>B}}\frac{\mathrm{Z_A Z_B}}{|\mathrm{R_A} - \mathrm{R_B}|} \tag{1.7}$$

In what follows, we will focus on how to solve the electronic problem, Eq.1.6. On refering to $\widehat{\mathrm{H}}_{\mathrm{elec}}$ and Ψ_{elec}, we will drop the subscript elec.

1.1 The Hartree-Fock aproximation

The Hartree-Fock (HF) approximation is the simplest approach to solve Eq.1.6. This method supposes that the electronic wave function Ψ is given by an antisymmetrized product of N spinorbitals, $\phi_i(x)$, known as Slater determinant

$$\Psi_{\mathrm{HF}} = \frac{1}{\sqrt{\mathrm{N!}}} \begin{vmatrix} \phi_1(x_1) & \phi_2(x_1) & \dots & \phi_N(x_1) \\ \phi_1(x_2) & \phi_2(x_2) & \dots & \phi_N(x_2) \\ \vdots & \vdots & \vdots & \vdots \\ \phi_1(x_N) & \phi_2(x_N) & \dots & \phi_N(x_N) \end{vmatrix} \tag{1.8}$$

The determinantal form of Ψ_{HF} ensures that the Pauli principle is satisfied. The HF approximation is a variational method which searchs for that set of orthonomalized spin orbitals which minimizes the electronic energy of the system. The expectation value of the energy is given by

$$\mathrm{E_{HF}} = \langle \Psi_{\mathrm{HF}} | \hat{\mathrm{H}} | \Psi_{\mathrm{HF}} \rangle = \sum_{\mathrm{i}} \mathrm{h_i} + \frac{1}{2} \sum_{\mathrm{i}} \sum_{\mathrm{j}} (\mathrm{J_{ij}} - \mathrm{K_{ij}}), \tag{1.9}$$

where

$$\mathrm{h_i} = \int \phi_{\mathrm{i}}^*(\mathrm{x}) \left[-\frac{1}{2} \nabla_{\mathrm{i}}^2 - \sum_{\mathrm{A}=1}^{\mathrm{M}} \frac{\mathrm{Z_A}}{|\mathrm{r_i} - \mathrm{R_A}|} \right] \phi_{\mathrm{i}}(\mathrm{x}) \mathrm{dx} \tag{1.10}$$

$$\mathrm{J_{ij}} = \int \int \phi_{\mathrm{i}}(\mathrm{x_1}) \phi_{\mathrm{i}}^*(\mathrm{x_1}) \frac{1}{\mathrm{r_{12}}} \phi_{\mathrm{j}}(\mathrm{x_2}) \phi_{\mathrm{j}}^*(\mathrm{x_2}) \mathrm{dx_1 dx_2} \tag{1.11}$$

$$\mathrm{K_{ij}} = \int \int \phi_{\mathrm{i}}(\mathrm{x_1}) \phi_{\mathrm{i}}^*(\mathrm{x_2}) \frac{1}{\mathrm{r_{12}}} \phi_{\mathrm{j}}(\mathrm{x_2}) \phi_{\mathrm{j}}^*(\mathrm{x_1}) \mathrm{dx_1 dx_2}. \tag{1.12}$$

The integrals $\mathrm{J_{ij}}$ and $\mathrm{K_{ij}}$ are called Coulomb and Exchange integrals respectively. The minimization of $\mathrm{E_{HF}}$ under the orthonormalization condition of the spin-orbitals, $\langle \phi_i | \phi_j \rangle = \delta_{ij}$ leads to the Hartree-Fock differential equations

$$\hat{\mathrm{f}}_{\mathrm{i}} \phi_{\mathrm{i}}(\mathrm{x}) = \sum_{\mathrm{j}} \epsilon_{\mathrm{ij}} \phi_{\mathrm{j}}(\mathrm{x}), \tag{1.13}$$

where $\widehat{\mathrm{f}}$ is the Fock operator

$$\hat{\mathrm{f}}_{\mathrm{i}} = \hat{\mathrm{h}}_{\mathrm{i}} + \sum_{\mathrm{j} \neq \mathrm{i}} [\hat{\mathrm{j}}_{\mathrm{j}} - \hat{\mathrm{k}}_{\mathrm{j}}]. \tag{1.14}$$

In Eq. 1.14, $\hat{\mathrm{h}}_{\mathrm{i}}$ is a monoelectronic hamiltonian, describing the kinetic and potential energy of one electron in the field of the nuclei

$$\hat{\mathrm{h}}_{\mathrm{i}} = -\frac{1}{2} \nabla_{\mathrm{i}}^2 - \sum_{\mathrm{A}} \frac{\mathrm{Z_A}}{|\mathrm{r_i} - \mathrm{R_A}|}, \tag{1.15}$$

$\hat{\mathrm{j}}$ is a local operator known as coulomb operator

$$\hat{\mathrm{j_k}}(\mathrm{x_1})\phi_\mathrm{i}(\mathrm{x_1}) = \int [\phi_\mathrm{k}^*(\mathrm{x_2})\frac{1}{\mathrm{r_{12}}}\phi_\mathrm{k}(\mathrm{x_2})]\mathrm{dx_2}\phi_\mathrm{i}(\mathrm{x_1}) \tag{1.16}$$

and $\hat{\mathrm{k}}$ is a non-local operator knows as exchange operator

$$\hat{\mathrm{k_k}}(\mathrm{x_1})\phi_\mathrm{i}(\mathrm{x_1}) = \int [\phi_\mathrm{k}^*(\mathrm{x_2})\frac{1}{\mathrm{r_{12}}}\phi_\mathrm{i}(\mathrm{x_2})]\mathrm{dx_2}\phi_\mathrm{k}(\mathrm{x_1}). \tag{1.17}$$

It is possible to take advantage of the invariance of the determinants and the Fock operator under unitary transformations of the orbitals and transform Eq. 1.13 into an eigenvalue equation of the form 1.3. First, Eq. 1.14 may be written in the matrix form

$$\mathrm{f}\phi = \epsilon\phi. \tag{1.18}$$

Now, since ϵ is a Hermitian matrix, it may be diagonalized by a unitary matrix U. Defining a new set of orbitals, $\bar{\phi} = \phi\mathrm{U}$, Eq. 1.13 may be written as $\mathrm{f}\bar{\phi} = \bar{\epsilon}\bar{\phi}$, being $\bar{\epsilon}$ diagonal. After this unitary approximation, we drop the bar and each spin-orbital satisfies:

$$\mathrm{f_i}\phi_\mathrm{i} = \epsilon_\mathrm{i}\phi_\mathrm{i} \tag{1.19}$$

These equations are known as the canonical Hartee-Fock equations and $\{\phi_\mathrm{i}\}$ are called the canonical Hartree-Fock orbitals with orbital energies $\{\epsilon_\mathrm{i}\}$. Under the canonical formulation, it is clear that the HF method is an independent-particle model, in the sense each spin orbital is an eigenfunction of an effective one-electron operator ($\hat{\mathrm{f}}_\mathrm{i}$). The electron interactions are only taken into account in an averaged form, i.e. each electron does not feel the instantaneous field generated by the remaining N-1 electrons of the system, but an averaged field given by the coulomb and exchange operators. The Hartree-Fock energy may be recovered from the orbital energies as

$$\mathrm{E_{HF}} = \sum_\mathrm{i} \epsilon_\mathrm{i} - \frac{1}{2}\sum_\mathrm{i,j}^\mathrm{N} \mathrm{J_{ij}} - \mathrm{K_{ij}}. \tag{1.20}$$

The second term disccounts the electronic repulsion energy that is counted twice in $\sum_i \epsilon_i$.

The HF equations must be solved by an iterative procedure known as self consisted field (SCF) method. The Fock operator depends on the spin-orbitals, but these functions are the solutions of the problem. Consequently, an initial guess for these spin-orbitals is needed. Then, the $\hat{\mathrm{f}}$ operator and the spin-orbitals are iteratively updated until the convergence in the ϵ_i and ϕ_i is reached.

1.2 Configurations Interaction

Despite the elegance and simplicity of the Hartree-Fock approximation, it does not take into account a fundamental property: the electron correlation. Although the electron

correlation supposes a little amount of the total energy of the system, it is essential for an accurate description of the electronic structure. The correlation energy (E_{corr}) is defined as the difference between the exact non-relativistic energy of the system and the Hartree-Fock energy:

$$E_{corr} = E - E_{HF}. \tag{1.21}$$

The Configuration Interactions (CI) method is the next step for improving the electronic structure description. The wave function is expanded in terms of a set of Slater determinants(D_i)

$$\Psi_o = \sum_i C_i D_i \tag{1.22}$$

$$D_i = \frac{1}{\sqrt{N!}} |\phi_{i_1}(x_1) \dots \phi_{i_N}(x_N)| \tag{1.23}$$

where $\{\phi\}$ is a set of M spin orbitals, ϕ_{i_1}, ϕ_{i_2},...,ϕ_{i_N} is the subset of $N < M$ spin orbitals used to construct the determinant D_i, and C_i are coefficients obtained variationally by minimizing the total energy $E_o = \langle \Psi_o | H | \Psi_o \rangle$. When all possible independent combinations of determinants are included in the expansion 1.22 the method is called *full* CI and it is the exact solution for a given basis set $\{\phi\}$. However, this limit is computationally very demanding, being only possible to perform *full CI* calculations for relatively small systems. The CI expansion is usually truncated at a given excitation level, giving a hierarchy of methods: CIS (includes all single excitations), CISD (includes all single and double excitations),... The CISD is the most usual truncation, since single and doubly excitations are the most important to lowering the ground state energy.

1.2.1 CI matrix

The CI energy is obtained by diagonalizing the matrix of the electronic Hamiltonian in the basis of the Slater determinants. To show the structure of this CI matrix, we express Ψ_o in a symbolic form

$$|\Psi_o\rangle = c_o|\Phi_o\rangle + c_S|S\rangle + c_D|D\rangle + c_T|T\rangle + \dots, \tag{1.24}$$

where $|\Phi_o\rangle$ is the Hartree-Fock wavefunction, $|S\rangle$ is the set of single excitations, $|D\rangle$ the set of double excitations and so on. The Brillouin's theorem and the Slater rules simplify the structure of the CI matrix.

Brillouin's Theorem. *Singly excited determinants will not interact directly with a reference Hartree-Fock determinant.*

This theorem cancels all the elements $\langle \Phi_o | H | S \rangle$. The Slater rules cancel all that matrix elements which couple two determinants that differ in more than two spin orbitals, i.e.,$\langle \Phi_o | H | T \rangle, \langle S | H | Q \rangle, \dots$. The CI matrix takes then a block structure

$$\begin{bmatrix} \langle \Phi_o|H|\Phi_o\rangle & 0 & \langle \Phi_o|H|D\rangle & 0 & 0 & \dots \\ 0 & \langle S|H|S\rangle & \langle S|H|D\rangle & \langle S|H|T\rangle & 0 & \dots \\ \langle D|H|\Phi_o\rangle & \langle D|H|S\rangle & \langle D|H|D\rangle & \langle D|H|T\rangle & \langle D|H|Q\rangle & \dots \\ \vdots & \vdots & \vdots & \vdots & \vdots & \dots \end{bmatrix}$$

1.2.2 Correlation energy

The correlation energy E_{corr} was defined in Eq. 1.21. In this section, we will show how to recover it at the *full CI* for the ground state of a molecular system. First, we write again Eq. 1.24 in more detail.

$$|\Psi_o\rangle = |\Phi_o\rangle + \sum_{ar} c_a^r |\Phi_a^r\rangle + \sum_{a<b,r<s} c_{ab}^{rs} |\Phi_{ab}^{rs}\rangle + \dots \tag{1.25}$$

where $|\Phi_a^r\rangle$ means a determinant created replacing the spin orbital r by the spin orbital a in $|\Psi_o\rangle$, $|\Phi_{ab}^{rs}\rangle$ a determinant created replacing the spin orbitals r and s by the spin orbitals a and b, respectively, and so on. Now, we impose an intermediate normalization condition

$$\langle \Psi_o | \Phi_o \rangle = 1. \tag{1.26}$$

The greater the contribution of the HF configuration to $|\Psi_o\rangle$, the more exact the HF approximation is. Similarly to the HF case, the ground state energy E_o is the solution of the equation:

$$H|\Psi_o\rangle = E_o|\Psi_o\rangle. \tag{1.27}$$

Applying the correlation energy definition (Eq. 1.21), and multiplying both sides of the above equation by $\langle \Phi_o|$ we have

$$\langle \Phi_o | H - E_{HF} | \Psi_o \rangle = \langle \Phi_o | E_o - E_{HF} | \Psi_o \rangle = E_{corr} \tag{1.28}$$

where the intermediate condition was used. Combining the Brioullin's theorem and the Slater rules, E_{corr} becomes:

$$E_{corr} = \sum_{a<b,r<s} c_{ab}^{rs} \langle \Psi_o | H | \Psi_{ab}^{rs} \rangle. \tag{1.29}$$

With the intermediate normalization condition, the correlation energy is solely determined by the double excitations. The single excitations only contribute indirectly by coupling with the double excitations. Although third and higher excitations are also coupled, their weights in the CI wave function are much lower. That is why single and double truncation are the most employed.

1.3 Multiconfigurational Methods

CI calculations use canonical Hartree-Fock orbitals to construct configurations. Since virtual orbitals do not contribute to the HF energy, they are not optimized at this level of calculation. The philosophy of multiconfigurational methods (MCSCF) is to find the best choice for all the orbitals. In this approximation, the wave function is expanded in terms of a set of configurations, $\{|\Psi_i\rangle\}$,

$$|\Psi_{MCSCF}\rangle = \sum_i C_i |\Psi_i\rangle, \tag{1.30}$$

and, unlike the CI method, in which only C_i coefficients are optimized, in the MCSCF procedure both, the C_i and the orbitals that define the $|\Psi_i\rangle_i$ are optimized. This make the process much computationally demanding, limiting the number of configuration to be included in the calculation.The choice of the configurations depends on the chemistry of the problem. There isn't any "general recipe"to select the configurations.

The cost of MCSCF may be reduced by restring not only the orbitals to be included in each configuration, but the number of electrons to be excited from HF configuration. That is, the orbitals are split in two sets. One set, called frozen orbital, will have occupation two in all the configurations. The other set, call active, are allowed to have occupation lower than two. The active space is specified by the number of electrons to be excited (m) and the number of active orbital (n). This sort of MCSCF method is known as Complete Active Space Self Consisted Field (CASSCF). A CASSCF (m,n) means that all the configuration yield from distribute m electrons in n orbital, are included in the wave function.

1.4 Density Functional Theory

All of the methods described so far obtain the properties of the system from the wave function. However, this wave function is a complex object from which it is difficult to access to the desired chemical information. The Density Functional Theory (DFT) is a different approach that extracts, in principle, any property of the system, not from the wave function, but from a simpler object, the electron density ρ. The DFT machinery rests on the Hohenberg-Kohn theorems.

1.4.1 First Hohenberg-Kohn theorem

First Hohenberg-Kohn Theorem. *For any system of interacting particles in an external potential* $V_{ext}(r)$*, this potential is determined uniquely, except for a constant, by the ground state particle density* ρ*.*

From this theorem, it follows that since the hamiltonian of the system is fully determined by $V_{ext}(r)$, all the properties of the system are completely determined given ρ.

The proof of 1.4.1 is straightforward. Suppose that there were two different external potentials $V^{(1)}_{ext}(r)$ and $V^{(2)}_{ext}(r)$ which differ in more than a constant and which lead to the same ground state density $\rho(r)$. The two potentials lead to different hamiltonians , $\widehat{H}^{(1)}$ and $\widehat{H}^{(2)}$, with different ground state wave functions, $\Psi^{(1)}$ and $\Psi^{(2)}$, with the same ground state density. Since $\Psi^{(2)}$ is not the ground state of $\widehat{H}^{(1)}$, it follows that

$$E^{(1)} = \langle\Psi^{(1)}|\widehat{H}^{(1)}|\Psi^{(1)}\rangle < \langle\Psi^{(2)}|\widehat{H}^{(1)}|\Psi^{(2)}\rangle \tag{1.31}$$

It is supposed that the ground state is non-degenerate. Otherwise, is not possible to

assure the above inequality. The last term may be rewritten as

$$\langle\Psi^{(2)}|\widehat{\mathrm{H}}^{(1)}|\Psi^{(2)}\rangle = \langle\Psi^{(2)}|\widehat{\mathrm{H}}^{(2)}|\Psi^{(2)}\rangle + \langle\Psi^{(2)}|\widehat{\mathrm{H}}^{(1)} - \widehat{\mathrm{H}}^{(2)}|\Psi^{(2)}\rangle \quad (1.32)$$

$$= \mathrm{E}^{(2)} + \int \mathrm{dr}[\mathrm{V_{ext}}^{(1)}(\mathrm{r}) - \mathrm{V}^{(2)}_{\mathrm{ext}}(\mathrm{r})]\rho(\mathrm{r}) \quad (1.33)$$

so that

$$\mathrm{E}^{(1)} < \mathrm{E}^{(2)} + \int \mathrm{dr}[\mathrm{V}^{(1)}_{\mathrm{ext}}(\mathrm{r}) - \mathrm{V}^{(2)}_{\mathrm{ext}}(\mathrm{r})]\rho(\mathrm{r}) \quad (1.34)$$

Considering $\mathrm{E}^{(2)}$ in the same way as $\mathrm{E}^{(1)}$ leads to

$$\mathrm{E}^{(2)} < \mathrm{E}^{(1)} + \int \mathrm{dr}[\mathrm{V}^{(2)}_{\mathrm{ext}}(\mathrm{r}) - \mathrm{V}^{(1)}_{\mathrm{ext}}(\mathrm{r})]\rho(\mathrm{r}) \quad (1.35)$$

If the two equations are add together, yields a contradictory inequality $\mathrm{E}^{(1)} + \mathrm{E}^{(2)} < \mathrm{E}^{(1)} + \mathrm{E}^{(2)}$. This establishes the desired result: there cannot be two different external potentials differing by more than a constant which give rise to the same non-degenerate ground state charge state density.

1.4.2 Second Hohenberg-Kohn theorem

Second Hohenberg-Kohn Theorem. *A universal functional for the energy* $\mathrm{E}[\rho]$ *in term of the density* $\rho(\mathrm{r})$ *can be defined, valid for any external potential* $\mathrm{V_{ext}}(\mathrm{r})$. *For any particular* $\mathrm{V_{ext}}(\mathrm{r})$ *the exact ground state energy of the system is the global minimum value of this functional, and the density* $\rho(r)$ *that minimizes the functional is the exact ground state density.*

Since all the properties are determined by ρ, each property may be viewed as a functional of ρ.

$$\mathrm{E}[\rho] = \mathrm{F_{HK}}[\rho] + \int \mathrm{dr}\mathrm{V_{ext}}\rho(\mathrm{r}) + \mathrm{V_{NN}} \quad (1.36)$$

where $\mathrm{V_{NN}}$ is the interaction energy of the nuclei and $\mathrm{F_{HK}}$ is a universal functional of the density which contains the kinetic and interaction energy functionals,

$$\mathrm{F_{HK}}[\rho] = \mathrm{T}[\rho] + \mathrm{V_{ee}}[\rho] \quad (1.37)$$

Now considerer a system with ground state density $\rho^{(1)}$, corresponding to an external potential $\mathrm{V}^{(1)}_{\mathrm{ext}}$ and a wave function $\Psi^{(1)}$. The energy of the system is

$$\mathrm{E}^{(1)} = \mathrm{E_{HK}}[\rho^{(1)}] = \langle\Psi^{(1)}|\widehat{\mathrm{H}}^{(1)}|\Psi^{1}\rangle \quad (1.38)$$

Consider now a different density $\rho^{(2)}$, which corresponds to a different wave function $\Psi^{(2)}$. The variational principle assures that

$$\mathrm{E}^{1} = \langle\Psi^{(1)}|\widehat{\mathrm{H}}^{(1)}|\Psi^{(1)}\rangle < \langle\Psi^{(2)}|\widehat{\mathrm{H}}^{(1)}|\Psi^{(2)}\rangle, \quad (1.39)$$

so any trial density different from the exact gives an upper limit to the exact ground state energy. In the Hohenberg-Kohn original work, the search of densities was constrained to those densities associated with some external potential, V_{ext}. These densities are called *V-representable*. This condition may be relaxed by the *N-representability* constrain, introduced by Levy. A density is said to be N-representable if it derives from a well-behaved wave function and integrates to the number of electrons. The formulation given by Levy, not only replaces the *V-representability* constrain to *N-representability* constrain, but extends the Hohenberg-Kohn theorems to degenerated ground states.

From the second theorem of Hohenberg-Kohn it follows that, if F_{HK} is known, the ground state density and energy are available by minimization of the total energy of the system with respect to variation in the density. However, it is not known how to calculate F_{HK} from the density. The Kohn-Sham approach tackles this problem including the kinetic energy of a set of non-interacting electrons in terms of independent particle wave functions, in addition to interaction terms modelled as density functionals.

1.5 Density matrices and Related Functions

One of the postulates of quantum mechanics states that all the information of a molecular system is contained in the wave function. However, as theoretical methods grow in complexity the wave functions become progressively more diffuse objects. This is reason why, in the spirit of the Density Functional Theory (DFT), it is customary to replace the wave function by other more manageable mathematical functions. In this sense, reduced density matrices (RDMs) provide us with a feasible formalism to recover not only any property of the system but also get new insights of the collective behaviour of the electrons.

1.5.1 The Electron Distribution

The wave functions obtained by any of the methods described in the previous section are built with one electron bricks, the spin-orbitals, which describe regions of the space occupied by a single electron with a given spin. According to the statistical interpretation of quantum mechanics, only the square of the wave function has a true physical meaning. This means that, even though a spin-orbital by itself is not an observable, its square has a clear physical interpretation. Consider a single electron with spin α described by the orbital $\psi_a(\mathbf{r})$. Its wave function is then given by $\phi_a(\mathbf{x}) = \psi_a(\mathbf{r})\alpha(\sigma)$, and the probability of finding it in the volume element $d\mathbf{r}$ placed at the point $\mathbf{r}$ and with a spin value between σ and $\sigma + d\sigma$ is given by

$$\rho(\mathbf{x})d\mathbf{x} = |\phi_a(\mathbf{x})|^2 d\mathbf{x} = |\psi_a|^2 |\alpha(\sigma)|^2 d\mathbf{r}d\sigma \tag{1.40}$$

The probability of finding the electron in the volume element $d\mathbf{r}$ with any spin is obtainend by integrating only the spin variable σ:

$$P(\mathbf{r})d\mathbf{r} = \int \rho(\mathbf{x})d\sigma = d\mathbf{r}\int |\phi_a(\mathbf{x})|^2 d\sigma \tag{1.41}$$

The functions $\rho(\mathbf{x})$ and $P(\mathbf{r})$ are then probability densities. They can be generalized to the case of many electron systems described by general wave functions $\Psi(\mathbf{x}_1, \mathbf{x}_2, \ldots, \mathbf{x}_n)$. The probability of finding an electron in a volume element $d\mathbf{x}_1$ at $\mathbf{x}_1$, another electron in a volume element $d\mathbf{x}_2$ at $\mathbf{x}_2$, and so on is given by

$$\Psi(\mathbf{x}_1, \mathbf{x}_2, \ldots, \mathbf{x}_N)\Psi^*(\mathbf{x}_1, \mathbf{x}_2, \ldots, \mathbf{x}_N)d\mathbf{x}_1 d\mathbf{x}_2 \ldots d\mathbf{x}_N \tag{1.42}$$

If $\Psi(\mathbf{x}_1, \mathbf{x}_2, \ldots, \mathbf{x}_N)$ is normalized, the electron distribution 1.42 satisfies

$$\int \Psi(\mathbf{x}_1, \mathbf{x}_2, \ldots, \mathbf{x}_N)\Psi^*(\mathbf{x}_1, \mathbf{x}_2, \ldots, \mathbf{x}_N)d\mathbf{x}_1 d\mathbf{x}_2 \ldots d\mathbf{x}_N = 1 \tag{1.43}$$

It is also possible to obtain the probability of finding a set of n electrons in the volume element $d\mathbf{x}_1 d\mathbf{x}_2 \ldots d\mathbf{x}_n$ at the point $\mathbf{x}_1\mathbf{x}_2 \ldots \mathbf{x}_n$ by integrating the spatial and spin variables of the remaining $N - n$ electrons

$$d\mathbf{x}_1 d\mathbf{x}_2 \ldots d\mathbf{x}_n \int \Psi(\mathbf{x}_1, \mathbf{x}_2, \ldots, \mathbf{x}_N)\Psi^*(\mathbf{x}_1, \mathbf{x}_2, \ldots, \mathbf{x}_N)d\mathbf{x}_{n+1} \ldots d\mathbf{x}_N. \tag{1.44}$$

We define the probability density $\rho_n(\mathbf{x}_1, \ldots, \mathbf{x}_n)$ as the integral in the above expression multiplied by the normalization factor $\binom{N}{n} n!$:

$$\rho_n(\mathbf{x}_1, \ldots, \mathbf{x}_n) = \binom{N}{n} n! \int \Psi(\mathbf{x}_1, \mathbf{x}_2, \ldots, \mathbf{x}_N) \Psi^*(\mathbf{x}_1, \mathbf{x}_2, \ldots, \mathbf{x}_N) d\mathbf{x}_{n+1} \ldots d\mathbf{x}_N \quad (1.45)$$

Similarly to Eq.1.41, the spinless counterpart of this probability density may be obtained by integrating the spin variables, yielding the spinless probability density

$$\rho_n(\mathbf{r}_1, \ldots, \mathbf{r}_n) = \int \rho_n(\mathbf{x}_1, \ldots, \mathbf{x}_n) d\sigma_1 \ldots d\sigma_n. \quad (1.46)$$

For $n = 1$, $\rho_n(\mathbf{r}_1, \ldots, \mathbf{r}_n)$ becomes the ordinary electron density $\rho(\mathbf{r})$, used in DFT calculations and obtained by X-ray crystallography experiments. For $n = 2$, the so-called pair density, $\rho_2(\mathbf{r}_1, \mathbf{r}_2)$, is obtained. All the ρ^n are normalized to the n-tuple of electrons

$$\int \rho_n(\mathbf{r}_1, \ldots, \mathbf{r}_n) d\mathbf{r}_1, \ldots, d\mathbf{r}_n = \binom{N}{n} n!, \quad (1.47)$$

with the particular cases for $n = 1$,

$$\int \rho_1(\mathbf{r}_1) d\mathbf{r}_1 = N, \quad (1.48)$$

and $n = 2$,

$$\int \rho_2(\mathbf{r}_1, \mathbf{r}_2) d\mathbf{r}_1 d\mathbf{r}_2 = N(N-1). \quad (1.49)$$

1.6 Reduced Density Matrices

In order to evaluate the average value of any observable, we introduce here the concept of reduced density matrix (RDM). Given an N-electron system, characterized by a normalized wave function Ψ, the n-order reduced density matrix (n-RDM) is defined as

$$\rho_n(\mathbf{x}_1, \mathbf{x}_2, ..., \mathbf{x}_n; \mathbf{x}'_1, \mathbf{x}'_2, ..., \mathbf{x}'_n) = \binom{N}{n} n! \int \Psi(\mathbf{x}_1, \mathbf{x}_2, ..., \mathbf{x}_n, ..., \mathbf{x}_N) \times$$

$$\Psi^*(\mathbf{x}'_1, \mathbf{x}'_2, ..., \mathbf{x}'_n, ..., \mathbf{x}_N) d\mathbf{x}_{i>n}. \quad (1.50)$$

n-RDMs are Hermitian and antisymmetric in each set of indices, so that

$$\rho_n(\mathbf{x}_1, \mathbf{x}_2, ..., \mathbf{x}_n; \mathbf{x}'_1, \mathbf{x}'_2, ..., \mathbf{x}'_n) = \rho_n^*(\mathbf{x}'_1, \mathbf{x}'_2, ..., \mathbf{x}'_n; \mathbf{x}_1, \mathbf{x}_2, ..., \mathbf{x}_n) \quad (1.51)$$

$$\rho_n(\mathbf{x}_1, \mathbf{x}_2, ..., \mathbf{x}_i, \mathbf{x}_j, ..., \mathbf{x}_n; \mathbf{x}'_1, \mathbf{x}'_2, ..., \mathbf{x}'_n) =$$
$$-\rho_n(\mathbf{x}_1, \mathbf{x}_2, ..., \mathbf{x}_j, \mathbf{x}_i, ..., \mathbf{x}_n; \mathbf{x}'_1, \mathbf{x}'_2, ..., \mathbf{x}'_i, \mathbf{x}'_j, ..., \mathbf{x}'_n). \quad (1.52)$$

By recurrence, it is possible to obtain lower order densities from the higher ones

$$\rho_{n-1}(\mathbf{x}_1,\ldots,\mathbf{x}_{n-1};\mathbf{x'}_1,\ldots,\mathbf{x'}_{n-1}) = \frac{1}{N-n+1}\int \rho_n(\mathbf{x}_1,\ldots,\mathbf{x}_n;\mathbf{x'}_1,\ldots,\mathbf{x'}_n)d\mathbf{x}_n \tag{1.53}$$

As we have announced at the beginning of this section, the formulation given in Eq.1.50 allow us to express the average value of any n-electrons operator in terms of n-RDMs. As an example, the expectation value of a one electron operator $\widehat{A}$ is given by

$$\langle\widehat{A}\rangle = N\int_{\mathbf{x_1}=\mathbf{x'_1}} \Psi(\mathbf{x}_1,\ldots,\mathbf{x}_N)\widehat{A}\Psi^*(\mathbf{x'}_1,\ldots,\mathbf{x'}_N)d\mathbf{x}_1,\ldots,d\mathbf{x}_N \tag{1.54}$$

$$= \int_{\mathbf{x_1}=\mathbf{x'_1}} \widehat{A}\rho_1(\mathbf{x}_1;\mathbf{x'}_1)d\mathbf{x}_1. \tag{1.55}$$

The probability densities or distributions, introduced in Eq.1.45, are just the diagonal elements of the n-RDMs

$$\rho_n(\mathbf{x}_1,\mathbf{x}_2,\ldots,\mathbf{x}_n;\mathbf{x'}_1,\mathbf{x'}_2,\ldots,\mathbf{x'}_n)|_{\mathbf{x}=\mathbf{x'}} = \rho_n(\mathbf{x}_1,\mathbf{x}_2,\ldots,\mathbf{x}_n) \tag{1.56}$$

In what follows, we will only focus in the diagonal and spinless part of n-RDMs, so unless they were necessary, we will drop the primed variables.

1.6.1 Cumulants from n-RDMs

The n-RDMs defined above have a part that can not be expressed in terms of RDMs of orders lower than n. These terms are known as cumulant densities matrices. The n^{th} order cumulant density matrix (n-CDM) is said to be the irreducible part of the n-RDM, and it contains the n-electrons correlation of the system. As we will see, to find explicit expressions for the n-CDMs is essential to obtain chemical bonding indicators at the HF and correlated levels of calculation. From the diagonal and spinless RDM defined in Eq 1.46, the explicit formulas for the first four CDMs are the following (See Appendix)

$$\rho^1_C(\mathbf{r}_1) = \rho_1(\mathbf{r}_1) \tag{1.57}$$

$$\rho^2_C(\mathbf{r}_1,\mathbf{r}_2) = \rho_1(\mathbf{r}_1)\rho_1(\mathbf{r}_2) - \rho_2(\mathbf{r}_1,\mathbf{r}_2) \tag{1.58}$$

$$\rho^3_C(\mathbf{r}_1,\mathbf{r}_2,\mathbf{r}_3) = \rho_1\rho_2\rho_3 - \frac{1}{2}\hat{S}\rho_1\rho_{23} + \frac{1}{2}\rho_{123}, \quad \text{and} \tag{1.59}$$

$$\rho^4_C(\mathbf{r}_1,\mathbf{r}_2,\mathbf{r}_3,\mathbf{r}_4) = \rho_1\rho_2\rho_3\rho_4 - \frac{1}{3}\hat{S}\rho_1\rho_2\rho_{34} + \frac{1}{6}\hat{S}\rho_1\rho_{234} + \frac{1}{6}\hat{S}\rho_{12}\rho_{34} - \frac{1}{6}\rho_{1234}, \tag{1.60}$$

where

$$\hat{S}\rho_1\rho_{23} = \rho_1\rho_{23} + \rho_2\rho_{13} + \rho_3\rho_{12} \tag{1.61}$$

$$\hat{S}\rho_1\rho_2\rho_{34} = \rho_1\rho_2\rho_{34} + \rho_1\rho_3\rho_{24} + \rho_1\rho_4\rho_{23} + \rho_2\rho_3\rho_{14} + \rho_2\rho_4\rho_{13} + \rho_3\rho_4\rho_{12} \tag{1.62}$$

$$\hat{S}\rho_1\rho_{234} = \rho_1\rho_{234} + \rho_2\rho_{134} + \rho_3\rho_{124} + \rho_4\rho_{123} \tag{1.63}$$

$$\hat{S}\rho_{12}\rho_{34} = \rho_{12}\rho_{34} + \rho_{13}\rho_{24} + \rho_{14}\rho_{23} \tag{1.64}$$

are fully symmetrized products ,and ρ_i, ρ_{ij}, ρ_{ijk}, and ρ_{ijkl} abbreviations for $\rho_1(\mathbf{r}_i)$, $\rho_2(\mathbf{r}_i, \mathbf{r}_j)$, $\rho_3(\mathbf{r}_i, \mathbf{r}_j, \mathbf{r}_k)$, and $\rho_4(\mathbf{r}_i, \mathbf{r}_j, \mathbf{r}_k, \mathbf{r}_l)$, respectively. In applying nCDMs to the chemical bond theory, their recursivity will play a key role

$$\rho_c^{n-1}(\mathbf{r}_1, \ldots, \mathbf{r}_{n-1}) = \int \rho_C^n(\mathbf{r}_1, \ldots, \mathbf{r}_{n-1}, \mathbf{r}_n) d\mathbf{r}_n \tag{1.65}$$

By a successive application of Equation 1.65, the number of electrons is recovered

$$\int \rho_c^n(\mathbf{r}_1, ..., \mathbf{r}_n)\, d\mathbf{r}_1 ... d\mathbf{r}_n = N \tag{1.66}$$

1.6.2 nCDMs at single determinant level

Although the Eqs.1.57, 1.58, 1.59, and 1.60 are valid for single (SDW) and multideterminant wave functions (MDW), as a pedagogical case, we apply these equations to the former case. The n-RDMs at the SD level may be obtained through the Fock-Dirac expansion

$$\rho_n(\mathbf{x}_1, \ldots, \mathbf{x}_n) = \begin{vmatrix} (1,1) & (1,2) & \ldots & (1,n) \\ (2,1) & (2,2) & \ldots & (2,n) \\ \vdots & \vdots & \ddots & \vdots \\ (n,1) & (n,2) & \ldots & (n,n) \end{vmatrix}, \tag{1.67}$$

where (i,j) is an abbreviated notation for the non-diagonal first-order RDM, $\rho_1(\mathbf{x}_i, \mathbf{x}_j)$. Only $(n-1)!$ of the $n!$ products of the form $\pm(1,i_1)(2,i_2)\ldots(n,i_n)$, where $(i_1, \ldots, i_n)$ is a permutation of $(1, \ldots, n)$ do not contain (i_1, i_1) elements, so they contribute to the irreducible part of n-RDM. For instance, the 3-RDM is given by

$$\begin{aligned} \rho_3(\mathbf{x}_1, \mathbf{x}_2, \mathbf{x}_3) &= (1,1)(2,2)(3,3) + (1,2)(2,3)(3,1) + (1,3)(3,2)(2,1) \\ &- (1,3)(2,2)(3,1) - (1,2)(2,1)(3,3) - (1,1)(2,3)(3,2) \end{aligned} \tag{1.68}$$

From these, only the 2$^{\text{nd}}$ and the 3$^{\text{rd}}$ ones contribute to ρ_C^3:

$$\rho_C^3(\mathbf{x}_1, \mathbf{x}_2, \mathbf{x}_3) = \frac{1}{2!}\left[(1,2)(2,3)(3,1) + (1,3)(3,2)(2,1)\right]. \tag{1.69}$$

The numerical factor is always $1/(n-1)!$, which coincides (in absolute value) with the coefficient of ρ_n in the expansion of ρ_C^n. $(n-1)!$ is the number of forms in which the circuit $1 \to a \to b \to \cdots \to 1$ can be travelled. For $n = 3$, there are only the $2! = 2$ possibilities that appear in Eq. 1.69: $1 \to 2 \to 3 \to 1$ (clockwise) and $1 \to 3 \to 2 \to 1$ (anticlockwise). However, for $n = 4$ we have $(1 \to 2 \to 3 \to 4 \to 1)$, $(1 \to 2 \to 4 \to 3 \to 1)$, $(1 \to 3 \to 2 \to 4 \to 1)$, $(1 \to 3 \to 4 \to 2 \to 1)$, $(1 \to 4 \to 2 \to 3 \to 1)$, and $(1 \to 4 \to 3 \to 2 \to 1)$. Indeed, for each n (except $n = 2$) there are only $(n-1)!/2$ independent circuits if the direction of the arrows is irrelevant.

1.6.3 Pair density and electron correlation

We have seen in the previous section how the RMDs formalism supply us with a vast arsenal to face the electron distribution problem. Since Lewis proposed one of the first models of chemical bonding, many efforts have been conducted to treat to express his ideas in a quantum mechanical parlance. The pair density $\rho_2(\mathbf{r}_1, \mathbf{r}_2$ in Eq.1.49) is the cornerstone to understand the electron pairing proposed by Lewis 90 year ago. From Eq. 1.58, $\rho_2(\mathbf{r}_1, \mathbf{r}_2$ has the form

$$\rho_2(\mathbf{r}_1, \mathbf{r}_2) = \rho(\mathbf{r}_1)\rho(\mathbf{r}_2) - \rho_C^2(\mathbf{r}_1, \mathbf{r}_2) \tag{1.70}$$
$$\tag{1.71}$$

As we have mentioned, this function gives a measure of the probability of finding any pair of electrons at the points $\mathbf{r}_1$ and $\mathbf{r}_2$ no matter where the remaining electrons of the system are. With the aim to extract all the information contained in ρ_2, we will develop a population analysis based on the conditional probability P_{cond}, defined as the probability of finding an electron at $\mathbf{r}_2$ when it is known that the first electron or reference electron is placed at $\mathbf{r}_1$

$$P_{\text{cond}}(\mathbf{r}_1|\mathbf{r}_2) = \frac{\rho_2(\mathbf{r}_1, \mathbf{r}_2)}{\rho(\mathbf{r}_1)}, \tag{1.72}$$

Since the reference electron is arbitrary located at $\mathbf{r}_1$, P_{cond} integrates to $N-1$

$$\int P_{\text{cond}}(\mathbf{r}_1|\mathbf{r}_2)d\mathbf{r}_2 = N - 1 \tag{1.73}$$

To explore the pair correlation, the exchange-correlation hole is defined as the difference between the full electron density and the the conditional probability

$$h_{xc}(\mathbf{r}_1|\mathbf{r}_2) = \rho(\mathbf{r}_2) - P_{\text{cond}}(\mathbf{r}_1|\mathbf{r}_2) \tag{1.74}$$
$$= \frac{\rho_C^2(\mathbf{r}_1, \mathbf{r}_2)}{\rho(\mathbf{r}_1)} \tag{1.75}$$

The exchange-correlation hole give us a measure of the pair-correlation, attaining its minimum value in the limiting case of independent particles. In such case, the pair density is given by

$$\rho_2^{ind} = \frac{N-1}{N}\rho(\mathbf{r}_1)\rho(\mathbf{r}_2), \tag{1.76}$$

where the prefactor $(N-1)/N$ takes into account that, once one electron is located at $\mathbf{r}_1$, the density of the other should integrate to $N-1$. As it was announced in section 1.6.1, $\rho_C^2(\mathbf{r}_1, \mathbf{r}_2)$ gives also a measure of the pair-correlation. As the pair correlation increases, $\rho_2(\mathbf{r}_1, \mathbf{r}_2)$ decreases through the contribution of $\rho_C^2(\mathbf{r}_1, \mathbf{r}_2)$ and consequently a "hole" is generated in the pair density. h_{xc} may be understood as the measure of such "hole".

By means of h_{xc} it is not only possible to account for the total correlation, but also distinguish the correlation effects between electrons with the same and opposite spins:

$$h_{xc}(\mathbf{x}_1|\mathbf{x}_2) = h_{xc}^{\sigma_1=\sigma_2}(\mathbf{r}_1|\mathbf{r}_2) + h_{xc}^{\sigma_1\neq\sigma_2}(\mathbf{r}_1|\mathbf{r}_2) \tag{1.77}$$
$$= h_F(\mathbf{r}_1|\mathbf{r}_2) + h_C(\mathbf{r}_1|\mathbf{r}_2). \tag{1.78}$$

The first term in Eq 1.77 is known as the Fermi hole, and takes into account the correlation between electrons with the same spin (Fermi correlation), as a consequence of the exclusion principle. The second terms contains the correlation between electrons with opposite spins (Coulomb correlation) and it is known as the Coulomb hole. It is a consequence of the repulsion suffered by the electron due to its charge, no matter the spin. Some of the properties that h_{xc} satisfies are

$$\int d\mathbf{r}_1 h_F(\mathbf{r}_1|\mathbf{r}_2) = 1 \tag{1.79}$$

$$h_F(\mathbf{r}_1 \to \mathbf{r}_2|\mathbf{r}_2) = \rho(\mathbf{r}_1) \tag{1.80}$$

$$\int d\mathbf{x}_1 h_C(\mathbf{r}_1|\mathbf{r}_2) = 0. \tag{1.81}$$

The properties 1.79, 1.80, and 1.81 are a consequence of the independence of electrons with different spin. Due to orthogonality of the spin function, setting an electron with spin α (β), only generates a "hole" in the $\alpha(\beta)$ density. Note that, even in independent particle models such as the Hartee-Fock method, the Fermi correlation remains, avoiding the cancellation of the Fermi hole. By contrast, in such models, the coulombic contribution to the correlation is neglected.

2 Topology

We interrupt here the statistical analysis started in the previous section to present a different mathematical tool, the topological analysis. Topological approaches make use of the topology of any chemically relevant scalar field to split the real space in different regions. These approaches help us to leave the traditional analysis based on the Fock space and how molecular orbitals guard the space and replace them by orbital invariant analyses of real space.

2.1 The Gradient Vector Field

Given a scalar function defined in the real space $\mathcal{R}^3$, $\rho(r) = \rho(x, yz)$, the gradient vector field of ρ is defined as

$$\vec{\nabla}\rho = \mathbf{i}\frac{\partial\rho}{\partial x} + \mathbf{j}\frac{\partial\rho}{\partial y} + \mathbf{k}\frac{\partial\rho}{\partial z} = \mathbf{i}\rho_x + \mathbf{j}\rho_y + \mathbf{k}\rho_z. \tag{2.1}$$

The gradient vector field is represented through a set of lines, known as gradient paths, which are the solution of a first order differential equation:

$$\frac{dx(s)}{ds} = \nabla\rho(r(s)), \tag{2.2}$$

where the parameter s is the distance from some starting point s_1. By integration of Eq.2.2, we get the position of any point of the gradient path that passes through the reference point $r(s_1)$,

$$r(s) = r(s_1) + \int_{s_1}^{s} \nabla\rho(r(t))dt. \tag{2.3}$$

For each of the three directions of $\mathcal{R}^3$ we get a similar equation to 2.3. In the real space these gradient paths may be identified as trajectories of the gradient vector field $\vec{\nabla}\rho$. Some of their properties are:

1. Since the gradient vector always point in the direction of greatest increase in the scalar field, the trajectories of $\vec{\nabla}\rho$ are perpendicular to lines of constant value of ρ.

2. The vector $\vec{\nabla}\rho$ is tangent to its trajectory at each point $r(s)$.

3. Every trajectory must originate or terminate at a point where $\vec{\nabla}\rho$ vanishes or in the infinity.

4. Trajectories can not cross since $\vec{\nabla}\rho$ defines only one direction at each point $r(s)$.

Specially relevant to analyze the topology of ρ are those points where $\vec{\nabla}\rho$ vanishes, known as critical points (CPs):

$$\vec{\nabla}\rho = \mathbf{i}\frac{\partial\rho}{\partial x} + \mathbf{j}\frac{\partial\rho}{\partial y} + \mathbf{k}\frac{\partial\rho}{\partial z} = \mathbf{i}\rho_x + \mathbf{j}\rho_y + \mathbf{k}\rho_z = \vec{0}. \tag{2.4}$$

Each CP of ρ may be classified by means of the second derivatives. In $\mathcal{R}^3$, there are nine second derivatives of the form $\frac{\partial^2\rho}{\partial x_i \partial x_j}$, being x_i and x_j any given pair of axis. They may ordered to form a 3×3 matrix called the Hessian matrix of ρ, or simply, the Hessian of ρ. At any given point $\mathbf{x}_0$, this matrix has the form

$$\mathbf{H}(\mathbf{x} = \mathbf{x}_0) = \begin{pmatrix} \frac{\partial^2\rho}{\partial x^2} & \frac{\partial^2\rho}{\partial x \partial y} & \frac{\partial^2\rho}{\partial x \partial z} \\ \frac{\partial^2\rho}{\partial y \partial x} & \frac{\partial^2\rho}{\partial y^2} & \frac{\partial^2\rho}{\partial y \partial z} \\ \frac{\partial^2\rho}{\partial z \partial x} & \frac{\partial^2\rho}{\partial z \partial y} & \frac{\partial^2\rho}{\partial z^2} \end{pmatrix}_{\mathbf{x}=\mathbf{x_0}} . \tag{2.5}$$

$\mathbf{H}$ is a real and symmetric matrix and, as such, it can be diagonalized. The eigenvectors and the eigenvalues of $\mathbf{H}$ are the principal axes of curvature and the curvatures of ρ respectively. Since the three eigenvalues are real, they may be equal to zero. Any critical point of ρ may be classified by its rank (ω) and by its signature (σ). The former is defined as the number of non-zero curvatures, and the last as the sum of the signs of the eigenvalues. Then, any given CP is labelled by the pair of values (ω, σ). In $\mathcal{R}^3$ any CP with $\omega < 3$ is a degenerated critical point. The CPs of rank 3 may be classified as follows:

- (3,-3): All the curvatures are negative and ρ is a local maximum at the CP.
- (3,+3): All the curvature are positive and ρ is a local minimum at the CP.
- (3,-1): ρ is a maximum at the CP in the plane defined by the axes with negative curvature and is minimum along the axis with positive eigenvalue, perpendicular to the other two axes. It is called a type-I saddle point.
- (3,+1): ρ is a minimum at the CP in the plane defined by the axes with positive curvature and is maximum along the axis with negative eigenvalue, perpendicular to the other two axes. It is called a type-II saddle point.

Each CP has associated a basin, given by all the points which belong to any trajectory that born or die in such CP. Mathematically, the former set is known as α-limit and the second as ω-limit.

Analyzing the CPs of any chemical sound scalar field, such as the electron density, the electron localization function (ELF) or the molecular electrostatic potential (MEP), many insights on the electron structure may be obtained. In what follows, we are going to focus on the topology of the first of these fields, the electron density.

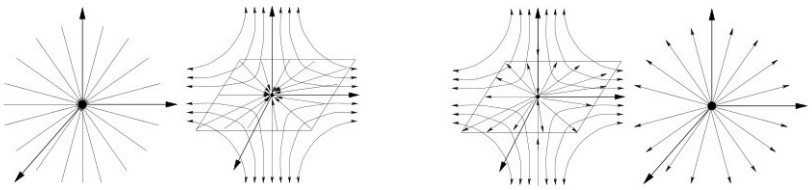

Figure 2.1: Gradients lines of the four kinds of critical point in $\mathcal{R}^3$:(3,-3),(3,-1),(3,+1),(3,+3).

2.2 Topology of the charge density

The gross form of the charge density, ρ, is dominated by cusps at the nuclear positions , due to the coalescence between the electron and the nucleus at such positions, as predicted by Kato[14]. This result has been widely proben not only with densities obtained by first principles, but also with experimental densities obtained by X-ray diffraction. The cusp condition avoids ρ to be a true differentiable field. However, it is possible to replace the cusp at nuclear positions by maxima, identifying the nuclear positions as (3,-3) CPs of ρ.

Mapping the density of many systems, it is found that all the saddle points of type I, CPs (3,-1), are placed between each pair of nuclear maxima, known then as bonding critical points (BCPs). For each BCP, there are a pair of gradient lines that terminate at the neighbouring maxima, known as bond path. The existence of a (3,-1) CP and its associated bond path lead to an accumulation of charge density between the linked nuclei. Then, it is said that both nuclei are bonded. From the display of the CPs of ρ, it is possible to define the molecular graph associated to a given configuration as the union of the bond paths.

By the inspection of more complex structures, (3,+1) and (3,+3) CPs are found. (3,+1) CPs appear is such structures where there is a planar region rounded by CPs, e.g. diborane presents a (3,+1) between the B atoms. (3,+1) CPs are known as ring critical points (Figure 2.2).

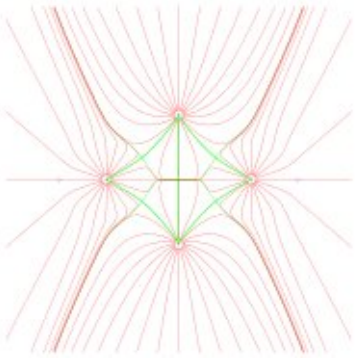

Figure 2.2: Molecular graph of the molecule of diborane.

The (3,+3) CPs are found in three-dimensions frames, such as cubane, and they are called cage critical points (Figure 2.3).

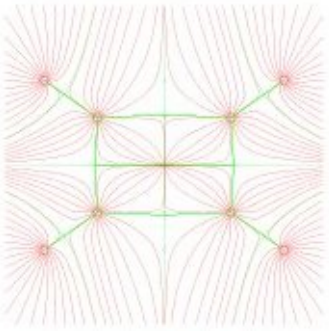

Figure 2.3: Molecular graph of the molecule of cubane.

The number and type of CPs which can coexist in a system with a finite number of nuclei are governed by the Morse relationship. In the case of ρ, this relation states that

$$\mathbf{n} - \mathbf{b} + \mathbf{r} - \mathbf{c} = \tau,$$

where n is the number of nuclei, b the number of bond paths, r the number of rings, and c the number of cages. τ is 1 in finite systems ,i.e molecules, and 0 in periodic systems, such as crystals. The collection (n, b, r, c) is called the characteristic set of the system.

2.3 Quantum Theory of Atoms in Molecule

The Quantum Theory of Atoms in Molecules (QTAIM) envisioned by R. F. W. Bader [3] is one of the most important theories for the analysis of the chemical bond in the real space. In the QTAIM the space is partitioned in disjoint regions, characterized by its surfaces: the flux lines generated by the gradient of the electron density do no traverse them. Mathematically this condition is expressed as

$$\nabla\rho(\mathbf{r}) \cdot \mathbf{n}(\mathbf{r}) = \mathbf{0}, \tag{2.6}$$

where $\mathbf{n}(\mathbf{r})$ is a normal vector to the surface at point the $\mathbf{r}$ and $\nabla\rho(\mathbf{r})$ is the gradient of $\rho(\mathbf{r})$ at $\mathbf{r}$. These regions, which partition the real space exhaustively ($\cup_{i=a}^{M}\Omega_a = \mathcal{R}^3$) do usually contain one and only one nucleus and are then called atomic basins (nucleus $\Leftrightarrow$ atomic basin). They can be identified as the atoms in the molecule.

2.3.1 Atomic Properties

Once the real space is exhaustively partitioned in atomic basins, it is possible to define the atomic average of an operator $\widehat{A}$ as

$$A_\Omega = \langle \widehat{A}_\Omega \rangle \;\; = \;\; \int_\Omega d\mathbf{r} \int d\mathbf{r}' \frac{N}{2} \big[\Psi^* \widehat{A} \Psi + (\widehat{A}\Psi)^* \Psi \big]. \tag{2.7}$$

An atomic property is therefore determined by the integration of a corresponding property density, ρ_A, over the basin of the atom

$$A_\Omega = \int_\Omega d\mathbf{r}\rho_A \tag{2.8}$$

where

$$\rho_A = \frac{N}{2}\int d\mathbf{r}'[\Psi^*\widehat{A}\Psi + (\widehat{A}\Psi)^*\Psi] \tag{2.9}$$

The above equations can also be expressed in terms of the reduced density matrices. If $\widehat{A}$ is a one-electron operator, Eq 2.8 becomes

$$A_\Omega = \int_\Omega d\mathbf{r}\widehat{A}(\mathbf{r};\mathbf{r}')\rho(\mathbf{r};\mathbf{r}')|_{\mathbf{r}=\mathbf{r}'}. \tag{2.10}$$

If $\widehat{A}$ is by contrast a two-electron operator

$$A_\Omega = \int_\Omega d\mathbf{r}_1\int_\Omega d\mathbf{r}_2\widehat{A}(\mathbf{r}_1;\mathbf{r}_2)\rho_2(\mathbf{r}_1;\mathbf{r}_2). \tag{2.11}$$

The most important consequence of the definition of an atomic property is that the average value of any observable may be partitioned in atomic contributions

$$\langle\widehat{A}\rangle = \sum_\Omega A_\Omega \tag{2.12}$$

Eq 2.12 states that each atom makes an additive contribution to any property of the system, recovering on the essential blocks of the chemistry: atoms and functional groups make recognizable contributions to the total properties of a system.

The simplest operator that we can integrate over a basin is the unity, $\widehat{A} = 1$. The property density associated to unity operator is the charge density and, from 2.9, the atomic population of atom Ω, defined as the average number of electrons in the basin Ω, N_Ω, is given by

$$N_\Omega = \int_\Omega \rho(\mathbf{r})d\mathbf{r} \tag{2.13}$$

Equivalently, from 2.11, the average number of pairs in the basin Ω may be cast as

$$D_2(\Omega,\Omega) = \int_\Omega\int_\Omega \rho_2(\mathbf{r}_1;\mathbf{r}_2)d\mathbf{r}_1d\mathbf{r}_2 \tag{2.14}$$

Any component of the energy of the system may be also partitioned into atomic contributions. For instance, one of the forms of the kinetic energy of the electrons in the basin A is given by

$$T_A = \int_{\Omega_A} d\mathbf{r}\nabla'\nabla\rho(\mathbf{r};\mathbf{r}')|_{\mathbf{r}=\mathbf{r}'}. \tag{2.15}$$

The electron-nucleus interaction may be partitioned as

$$V_{en}^{AB} = -\mathbf{Z}_B \int_{\Omega_A} \frac{\rho(\mathbf{r})}{|\mathbf{r} - \mathbf{R}_B|} d\mathbf{r} \tag{2.16}$$

where V_{en}^{AB} is the interaction between electrons in the basin A and the nucleus B. Note that $V_{en}^{AB} \neq V_{en}^{BA}$. Even if nucleus A and B were equal, if their basins were not identical both terms would be different. The electron-electron interaction may be cast as

$$V_{ee}^{AB} = \frac{1}{2} \int_{\Omega_A} \int_{\Omega_B} r_{12}^{-1} \rho_2(\mathbf{x}_1, \mathbf{x}_2) d\mathbf{x}_1 d\mathbf{x}_2 \tag{2.17}$$

where V_{ee}^{AB} is the electron repulsion between electrons in the basin A and the electrons in the basin B.

With the expressions given in Eqs. 2.15, 2.16, 2.17, the energy of atom A is defined as

$$E_A = T_A + V_{en}^{AA} + \sum_{B \neq A} V_{en}^{AB} + V_{ee}^{AA} + \sum_{B \neq A} V_{ee}^{AB}. \tag{2.18}$$

As an atomic property, the total energy E, may be recovered as the sum of all the atomic energies.

$$E = \sum_A E_A \tag{2.19}$$

This energetic partition is the source of the widely accepted IQA procedure [15], [16],[17]. IQA gathers appropriately the energetic terms in such a way that chemical intuition is recovered. Thus,

$$\begin{aligned} E &= \sum_A (T_A + V_{en}^{AA} + V_{ee}^{AA}) \\ &+ \sum_{A>B} (V_{nn}^{AB} + V_{en}^{BA} + V_{ee}^{AB}) \\ &= \sum_A E_{self}^A + \sum_{A>B} E_{int}^{AB} \end{aligned} \tag{2.20}$$

Separating intra-basin (intra-atomic) from inter-atomic terms, the total energy is split is self and interaction energies. When no interaction exits among atoms, E_{self}^A collapses over the *in vacuo* atomic energy. Taking an appropriate atomic reference, the deformation energy of the atom A is defined as $E_{def}^A = E_{self}^A - E_{ref}^A$, where E_{ref}^A is the energy of the atom A in its reference state. Now, the binding energy is defined as

$$E_{bind} = E - \sum_A E_{def}^A = \sum_A E_{def}^A + \sum_{A>B} E_{int}^{AB} \tag{2.21}$$

In this approach, the bonding may be understood as a balaced between deformation energies (usually positive) and interaction energies (overall negatives) . The partition of the 2RDM into Coulomb and exchange-correlation terms (Eq. 1.58) facilitates a meaningful rearrangement of the interaction energy, into the respective Coulomb and exchange-correlation parts. $V_{ee}^{AB} = V_{Coul}^{AB} + V_{xc}^{AB}$, and the classical component of the interaction energy is defined $V_{cl}^{AB} = (V_{nn}^{AB} + V_{en}^{AB} + V_{en}^{BA} + V_{Coul}^{AB})$.

3 Chemical bonding in real space

Understanding chemical bonding forms the undisputed foundation of chemistry. However, chemical bonds are not directly observables, so it is not possible to define any quantum mechanics operator associated with them (although Bader has claimed that a Bond Path operator exist [18]). These difficulties motivated quantum chemists to find different strategies to link classical (i.e. prequantum-mechanics) and quantum mechanical concepts. Many years after Lewis announced its model, Daudel [4] and co-workers searched how to divide the real space in disjoint regions or lodges such that they represent the most probable division of the physical space of a system into localized groups of electrons. These loges can be found, in principle, by minimizing the Shannon entropy, defined as

$$I(P_n, \Omega) = -\sum_n P_n(\Omega)\ln(P_n(\Omega)),$$

where $P_n(\Omega)$ is the probability of finding n electrons in the region (or lodge) Ω and the other $(N-n)$ in the complementary region $\Omega' = \mathcal{R}^3 - \Omega$:

$$P_n(\Omega) = \binom{N}{n} \int_{\mathbf{\Omega}} d\mathbf{r}_1 \dots d\mathbf{r}_n \int_{\mathbf{\Omega'}} d\mathbf{r}_{n+1} \dots d\mathbf{r}_N \rho_N(\mathbf{r}_1, \dots . \mathbf{r}_N). \tag{3.1}$$

Bader and Stephens showed in their seminal paper [10] that all the requirements for electron localization are contained in the electron (ρ_1) and pair (ρ_2) densities.

3.1 Pair density and electron localization

Given an exhaustive bipartition of the real space ($\Omega \cup \Omega' = \mathcal{R}^3$), defined by Bader's theory or another, the probability of finding n electron in one of such regions Ω and the remaining $N-n$ electrons in the complementary region $\Omega' = \mathcal{R}^3 - \Omega$ is given by Eq. 3.1. In terms of P_n, the average number of pairs in Ω is given by

$$D_2(\Omega, \Omega) \;=\; \int_\Omega \int_\Omega \rho_2(\mathbf{r}_1, \mathbf{r}_2) = \sum\nolimits_n P_n(\Omega) n(n-1). \tag{3.2}$$

From the cumulant expansion of 2RDM, $\rho_2(\mathbf{r}_1, \mathbf{r}_2) = \rho(\mathbf{r}_1)\rho(\mathbf{r}_2) - \rho_C^2(\mathbf{r}_1, \mathbf{r}_2)$, Eq. 3.2 becomes

$$D_2(\Omega, \Omega) = \langle N_\Omega \rangle^2 - \langle N_{\Omega,\Omega} \rangle \tag{3.3}$$

where

$$\langle N_\Omega \rangle = \int_\Omega d\mathbf{r}_1 \rho(\mathbf{r}_1) \tag{3.4}$$

and

$$\langle N_{\Omega,\Omega}\rangle = \int_\Omega d\mathbf{r}_1 \int_\Omega d\mathbf{r}_2 \rho_C^2(\mathbf{r}_1,\mathbf{r}_2). \tag{3.5}$$

The quantity $\langle N_{\Omega,\Omega}\rangle$ may be understood as a measure of the total correlation inside the region Ω, since it reduces the number of pairs created by an independent electron distribution. $\langle N_{\Omega,\Omega}\rangle$ is closely connected with the fluctuation in the population of Ω, defined as

$$\begin{aligned}\Lambda(\Omega) &= \sum_{n=0}^{N} P_n(\Omega)(n-\langle N_\Omega\rangle)^2 = \sum_{n=0}^{N} n^2 P_n(\Omega) - \sum_{n=0}^{N} n P_n(\Omega) \\ &= \langle N_\Omega^2\rangle - \langle N_\Omega\rangle^2. \end{aligned} \tag{3.6}$$

On the other hand, $D_2(\Omega,\Omega)$ in Eq. 3.3 may also be written as

$$D_2(\Omega,\Omega) = \sum\nolimits_n P_n(\Omega) n(n-1) = \langle N_\Omega^2\rangle - \langle N_\Omega\rangle. \tag{3.7}$$

From Eqs. 3.4 and 3.7, we have

$$\langle N_\Omega^2\rangle = \langle N_\Omega\rangle^2 + \langle N_\Omega\rangle - \langle N_{\Omega,\Omega}\rangle, \tag{3.8}$$

and substituting this equation in 3.6 we finally get

$$\Lambda(\Omega) = \langle N_\Omega\rangle - \langle N_{\Omega,\Omega}\rangle. \tag{3.9}$$

$\langle N_{\Omega,\Omega}\rangle$ decreases the fluctuation in the population of Ω, increasing the electron localization in such region. Due to this property this term receives the name of localization index. When $\langle N_{\Omega,\Omega}\rangle$ attains its maximum value, $\langle N_\Omega\rangle$, the fluctuation $\Lambda(\Omega)$ becomes zero, generating a situation of maximum localization. In such a case, the probability of finding n electrons in Ω, $P_n(\Omega)$, becomes one, $\langle N_\Omega\rangle$ is equal to n, and the average number of pairs in Ω is $\langle N_\Omega\rangle(\langle N_\Omega\rangle - 1)$. This limit situation is known as a pure pair population.

Similarly, one can measure the degree of localization of the electrons in two different regions Ω_1 and Ω_2 by determining the fluctuation in the population of the combined region $\Omega = \Omega_1 + \Omega_2$

$$\Lambda(\Omega) = \Lambda(\Omega_1) + \Lambda(\Omega_2) - 2\langle N_{\Omega_1,\Omega_2}\rangle \tag{3.10}$$

where

$$\langle N_{\Omega_1,\Omega_2}\rangle = \int_{\Omega_1} d\mathbf{r}_1 \int_{\Omega_2} d\mathbf{r}_2 \rho_C^2(\mathbf{r}_1,\mathbf{r}_2) \tag{3.11}$$

and $\Lambda(\Omega_1)$ and $\Lambda(\Omega_2)$ are given by Eq 3.6. The quantity $2\langle N_{\Omega_1,\Omega_2}\rangle$ is a measure of the extent to which electrons in Ω_1 are delocalized over Ω_2 and *viceversa* and it is known as delocalization index $\delta^{\Omega_1\Omega_2}$.

If these two regions complete the space, $\Omega_1 \cup \Omega_2 = \mathcal{R}^3$, one finds that

$$\langle N_{\Omega_1,\Omega_1}\rangle + \langle N_{\Omega_2,\Omega_2}\rangle + 2\langle N_{\Omega_1,\Omega_2}\rangle = N \tag{3.12}$$

Since for a closed system the number of electrons remains constant, maximizing the degree of localization in a given region leads to a minimization of the electron delocalization between different regions. The number of pairs that can be formed between electrons in different regions is given by

$$D_2(\Omega_1,\Omega_2) = \int_{\mathbf{\Omega}_1}\int_{\mathbf{\Omega}_2} \rho_2(\mathbf{r}_1,\mathbf{r}_2) = \langle N_{\Omega_1}\rangle\langle N_{\Omega_2}\rangle - \langle N_{\Omega_1,\Omega_2}\rangle \tag{3.13}$$

In the limit of pure pair population, $\langle N_{\Omega_1,\Omega_1}\rangle$ and $\langle N_{\Omega_2,\Omega_2}\rangle$ attain their maxima values, $\langle N_{\Omega_1}\rangle$ and $\langle N_{\Omega_2}\rangle$, respectively. In that case, the delocalization index, $2\langle N_{\Omega_1,\Omega_2}\rangle$, becomes zero and the electrons are perfectly localized in both regions. The number of pairs formed between the two regions, becomes from Eq 3.10 equal to the number of pairs that be formed with two sets of distinct objects.

If real space is partitioned into several regions, $\cup_{i=a}^{m}\Omega_a = \mathcal{R}^3$ $(m \geq 2)$, the above relations between the delocalization and localization indices may be generalized. For instance, Eq. 3.29 becomes

$$\sum_a \langle N_{aa}\rangle + 2\sum_{a\neq b}\langle N_{ab}\rangle = N, \tag{3.14}$$

where the indices $a, b, \ldots$ run over the basins. The definitions of localization and delocalization indices both together with Eqs 3.6 and 3.7 show how the inter and intra correlation may be described from the second order cumulant, $\rho_c^2(\mathbf{r}_1,\mathbf{r}_2)$. Indeed, $\rho_c^2(\mathbf{r}_1,\mathbf{r}_2)$ may be seen as a generator of 2-particle fluctuation in the electron distributions [19]. We shall see how all these concepts many be generalized, not only for two disjoint domains in the real space, but for any number $(m \geq 2)$ of regions by means of n^{th} order cumulants

3.2 Generalized population analysis

Given an exhaustive partition of real space, $\cup_{i=a}^{m}\Omega_a = \mathcal{R}^3$, , the properties of cumulants can be used to obtain a one basis partition of the electron density $\rho(\mathbf{r}) = \rho_C^1(\mathbf{r})$ from the second order cumulant $\rho_C^2(\mathbf{r}_1,\mathbf{r}_2)$

$$\rho_C^1(\mathbf{r}) = \sum_a^m \int_{\Omega_a} d\mathbf{r}_2 \rho_C^2(\mathbf{r},\mathbf{r}_2) = \sum_a^m \rho_a^1(\mathbf{r}), \tag{3.15}$$

Similarly, $\rho_C^n(\mathbf{r})$ allows for a $(n-1)$-basin partition of $\rho_C^1(\mathbf{r})$:

$$\rho_C^1(\mathbf{r}) = \sum_{ab}^m \rho_{ab}^1(\mathbf{r}) = \sum_{ab}^m \int_{\Omega_a} d\mathbf{r}_2 \int_{\Omega_b} d\mathbf{r}_3\, \rho_C^3(\mathbf{r},\mathbf{r}_2,\mathbf{r}_3), \tag{3.16}$$

$$\rho_C^1(\mathbf{r}) = \sum_{abc}^m \rho_{abc}^1(\mathbf{r}) = \sum_{abc}^m \int_{\Omega_a} d\mathbf{r}_2 \int_{\Omega_b} d\mathbf{r}_3 \int_{\Omega_c} d\mathbf{r}_4\, \rho_C^4(\mathbf{r},\mathbf{r}_2,\mathbf{r}_3,\mathbf{r}_4). \tag{3.17}$$

This partition of $\rho^1_C(\mathbf{r})$ into basins, pairs of basins, etc, may also be extended to higher CDMs:

$$\rho^2_C(\mathbf{r}_1,\mathbf{r}_2) = \sum_a^m \rho^2_{C,a}(\mathbf{r}_1,\mathbf{r}_2) = \sum_a^m \int_{\Omega_a} d\mathbf{r}_3 \rho^3_C(\mathbf{r}_1,\mathbf{r}_2,\mathbf{r}_3) \tag{3.18}$$

$$\rho^2_C(\mathbf{r}_1,\mathbf{r}_2) = \sum_{ab}^m \rho^2_{C,ab}(\mathbf{r}_1,\mathbf{r}_2) = \sum_{ab}^m \int_{\Omega_a} d\mathbf{r}_3 \int_{\Omega_b} d\mathbf{r}_4 \rho^4_C(\mathbf{r}_1,\mathbf{r}_2,\mathbf{r}_3,\mathbf{r}_4). \tag{3.19}$$

For each ρ^n_C, we can also integrate the n^{th} electron such that the result is a scalar depending only on the definition of the Ω_i basins:

$$\langle N_a \rangle = \int_{\Omega_a} d\mathbf{r}_1 \; \rho^1_C(\mathbf{r}_1), \tag{3.20}$$

$$\langle N_{ab} \rangle = \int_{\Omega_a} d\mathbf{r}_1 \int_{\Omega_b} d\mathbf{r}_2 \; \rho^2_C(\mathbf{r}_1,\mathbf{r}_2), \tag{3.21}$$

$$\langle N_{abc} \rangle = \int_{\Omega_a} d\mathbf{r}_1 \int_{\Omega_b} d\mathbf{r}_2 \int_{\Omega_c} d\mathbf{r}_3 \; \rho^3_C(\mathbf{r}_1,\mathbf{r}_2,\mathbf{r}_3), \tag{3.22}$$

$$\langle N_{abcd} \rangle = \int_{\Omega_a} d\mathbf{r}_1 \int_{\Omega_b} d\mathbf{r}_2 \int_{\Omega_c} d\mathbf{r}_3 \int_{\Omega_d} d\mathbf{r}_4 \; \rho^4_C(\mathbf{r}_1,\mathbf{r}_2,\mathbf{r}_3,\mathbf{r}_4). \tag{3.23}$$

Eq. 3.20 gives the average number of electrons in the basin Ω_a, $2\langle N_{ab}\rangle$ coincides with the localization index between basins Ω_a and Ω_b given in Eq 3.8. The n-center delocalization index can be defined as $n!\langle N_{abcd,\ldots,n}\rangle$ and denoted by $\delta^{abcd,\ldots,n}$. Eq. 3.11 may be generalized to a n center partition of the electron population

$$N = \sum\nolimits_a^m \langle N_a \rangle \tag{3.24}$$

$$\langle N_a \rangle = \langle N_{aa} \rangle + 2\sum\nolimits_{b\neq a}^m \langle N_{ab} \rangle \tag{3.25}$$

From the recursivity of cumulants, each the n-center partition of the first order density integrates to the corresponding n-center DI

$$\int \rho^1_a(\mathbf{r}) d\mathbf{r} = \langle N_a \rangle \tag{3.26}$$

$$\int \rho^1_{ab}(\mathbf{r}) d\mathbf{r} = \langle N_{ab} \rangle \tag{3.27}$$

$$\int \rho^1_{abc}(\mathbf{r}) d\mathbf{r} = \langle N_{abc} \rangle \tag{3.28}$$

Each of these generalized densities may re-written in a matrix notation with the unified expression

$$\rho^1_{abc\ldots}(\mathbf{r}) = \phi(\mathbf{r}) \mathbf{D}^{abc\ldots} \phi(\mathbf{r})^\dagger, \tag{3.29}$$

where the $\phi(\mathbf{r})$ matrix contains the set of occupied molecular orbitals (MOs) and $\mathbf{D}^{abc...}$ is a symmetric matrix. By diagonalization of $\mathbf{D}^{abc...}$, $\rho^1_{abc...}(\mathbf{r})$ may be expressed as sum of quadratic forms

$$\rho^1_{abc...}(\mathbf{r}) = \sum_i^N n_i^{abc...}(\psi_i^{abc...})^2, \tag{3.30}$$

where N is the number of occupied MOs, the set $\psi_i^{abc...}$ are the eigenvectors of $\mathbf{D}^{abc...}$ and $n_i^{abc...}$ its eigenvalues. Since the trace of $\mathbf{D}^{abc...}$ recovers the average populations $\langle N_{abc...}\rangle$, the n-center DI are connected with $n_i^{abc...}$ by

$$\sum_i^N n_i^{abc...} = \frac{\delta^{abc...}}{n!}. \tag{3.31}$$

The eigenvectors $\psi_i^{abc...}$ may be understood as effective one-electrons functions that contribute additively to the delocalization index between n centers. In the case of one center, the diagonalization of $\mathbf{D}^a$ leads to a set of orthonormal orbitals widely explored in the literature and known as domain natural orbitals (DNOs). This set may be either localized in the basin Ω_a or its complementary, or delocalized over different basins. It has been found that only such delocalized DNOs contribute to the bonding, describing effective quasiparticles that behave as statically independent particles [20]. From this probabilistic interpretation, the eigenvalue n_i^a may be understood as the probability that the effective electron $\psi_i^{a...}$ rests in the basin Ω_a [20]. When more than one basin is involved, the set of functions $\psi_i^{abc...}$ are known as Natural Adaptive Oribitals (NAdOs)[13].

As we did before, it is convenient at this moment to illustrate how to get the general expressions for the n-center bonding indices, $\langle N_{abc...}\rangle$, densities, $\rho^1_{abc...}(\mathbf{r})$, etc, for single-determinant wave functions (SDWs). The spinless non-diagonal elements of 1-RDM for a closed-shell SDW are given by

$$\rho^1(\mathbf{r}_i, \mathbf{r}_j) = \sum_{k=1}^{N/2} 2\phi_k(\mathbf{r}_i)\phi_k(\mathbf{r}_j). \tag{3.32}$$

Taking into account this expression and the orthogonality of α and β spin functions, the spinless 2-CDM, $\rho^2_C(\mathbf{r}_1, \mathbf{r}_2)$, is given by

$$\begin{aligned}
\rho^2_C(\mathbf{r}_1, \mathbf{r}_2) &= \int \rho^2_C(\mathbf{x}_1, \mathbf{x}_2) ds_1 ds_2 && (3.33)\\
&= \frac{1}{2}\rho^1(\mathbf{r}_1, \mathbf{r}_2)\rho^1(\mathbf{r}_2, \mathbf{r}_1) && (3.34)\\
&= \sum_{k,l}^{N/2} 2\phi_k(\mathbf{r}_1)\phi_k(\mathbf{r}_2)\phi_l(\mathbf{r}_2)\phi_l(\mathbf{r}_1). && (3.35)
\end{aligned}$$

The n-CDM with $n > 2$ including spin for SDWs is given by a linear combination of $(n-1)!$ terms of the form $(1ab\ldots1) = (1,a)(a,b)\ldots(c,1)$. Integrating the spin

coordinates one has

$$\int (1ab\ldots 1)\, ds_{i\leq n} = 2\sum_{kl\ldots m} \phi_k(\mathbf{r}_1)\phi_k(\mathbf{r}_a)\phi_l(\mathbf{r}_a)\phi_l(\mathbf{r}_b)\ldots\phi_m(\mathbf{r}_c)\phi_m(\mathbf{r}_1) \tag{3.36}$$

$$= 2^{1-n}\rho_1(\mathbf{r}^1,\mathbf{r}_a)\rho^1(\mathbf{r}_a,\mathbf{r}_b)\ldots\rho_1(\mathbf{r}_c,\mathbf{r}_1). \tag{3.37}$$

Finally, condensing the electrons 2, 3, ..., n into Ω_a, Ω_b, ..., Eq. 3.29 is obtained, with $\mathbf{D}^a$, $\mathbf{D}^{ab}$, $\mathbf{D}^{abc}$, ..., given now by

$$\left(\mathbf{D}^a\right)_{ij} = 2\left(\mathbf{S}^a\right)_{ij} \tag{3.38}$$

$$\left(\mathbf{D}^{ab}\right)_{ij} = \sum_{l=1}^{N/2}\left[\mathbf{S}^a_{il}\mathbf{S}^b_{lj} + \mathbf{S}^b_{il}\mathbf{S}^a_{lj}\right] \tag{3.39}$$

$$\left(\mathbf{D}^{abc}\right)_{ij} = \frac{1}{3}\sum_{l,m=1}^{N/2}\left[\mathbf{S}^a_{il}\mathbf{S}^b_{lm}\mathbf{S}^c_{mj} + \mathbf{S}^a_{il}\mathbf{S}^c_{lm}\mathbf{S}^b_{mj} + \ldots\right], \tag{3.40}$$

where $\mathbf{S}^\Omega_{kl}$ are the elements of the atomic overlap matrix (AOM)

$$\mathbf{S}^\Omega_{kl} = \int_\Omega \phi_k(\mathbf{r})\phi_l(\mathbf{r})d\mathbf{r}. \tag{3.41}$$

For the general case, we have

$$\left(\mathbf{D}^{\Omega_1\ldots\Omega_p}\right)_{ij} = \frac{2}{p!}\sum_{i_1 i_2\ldots i_{p-1}} \hat{S}_{\Omega_1\ldots\Omega_p}\left[\mathbf{S}^{\Omega_1}_{ii_1}\mathbf{S}^{\Omega_2}_{i_1 i_2}\mathbf{S}^{\Omega_3}_{i_2 i_3}\ldots\mathbf{S}^{\Omega_p}_{i_{p-1}j}\right]. \tag{3.42}$$

As we can see, $\mathbf{D}^{abc\ldots}$ is given in all the cases by a normalized and symmetrized product of AOMs.

Obtaining the bonding indices and $\rho^1_{abc\ldots}(\mathbf{r})$ in the case of multideterminant wave functions (MDWs) implies to compute the n-CDMs from RDMs, as it has been shown before, and integrate them over basins $\Omega_a, \Omega_b, \ldots$. In the results section, we shall calculate $\langle \mathrm{N}_{aa}\rangle$, $\langle \mathrm{N}_{ab}\rangle$, and two-center NAdOs of different molecular systems.

3.3 Reduced Density Gradient

We leave the cumulant expansion of the electron density to focus in other related function: the reduced density gradient (s). s is a well-known function in the DFT parlance. Its origen dates back to the generalized gradient contribution to the GGA exchange energy, E_x^{GGA} [21],

$$E_x^{GGA} - E_x^{LDA} = -\sum \int F(s)\rho^{4/3}(r)dr \tag{3.43}$$

where F(s) is a function of the reduced density gradient,s, for a given spin defined as

$$s = \frac{1}{C_F}\frac{|\nabla\rho|}{\rho^{4/3}}, \qquad C_F = 2(3\pi^2)^{1/3} \tag{3.44}$$

From the defintion of s (Eq. 3.44) becomes that s a is semipositive definite function ($s \geq 0$), attaining its minima at the critical points of the electron density ($\nabla\rho = 0$). It assumes large values in the exponentially decaying density far from the nuclei, where the denominator approaches to zero more rapidly than the numerator. By contrast, small values of s occurs close to the nuclei, due to the large values of the density in such regions.

The average value of the reduced density gradient $\langle s \rangle$ is a measure of the inhomogeneity of the system. For a homogeneous electron gas is exactly zero and it increases in leaving this reference system. In a real system, the roots of s occur , as aforementioned, at the CPs of ρ (nuclei, bonding critical points,...).

In 1991 Kohout, Savin and Preuss employed a similar function to s, $\frac{-|\nabla\rho|}{\rho}$ to resolve the atomic shell structure. In 1997 Zupan and co-workers, analyzing local and semilocal density functionals for the exchange-correlation energy, reported the capability of the reduced density gradient to describe atomic shell structures. However, not many applications of s to molecular systems were carried out at first, despite the success of their analysis. This situation has recently changed thanks to the fruitful analysis of long range interactions by means of s, which has motivated the ongoing of new bonding descriptors based on this function

3.3.1 Shell structure as described by s

The success of the reduced density gradient as an atomic shell descriptor is a consequence of the exponential decay of the electron density[22],[23]. For r $\to \infty$, the electron density of an atom is described by

$$\begin{aligned} \sqrt{\rho(r)} &\to r^{\kappa}e^{-\lambda r} \qquad \lambda = \sqrt{2IP} \\ \kappa &= \frac{(Z-N+1)}{(\lambda-1)} \end{aligned} \tag{3.45}$$

where IP is the ionization potential, Z the nuclear charge and N the number of electrons. For our purpose, let us suppose that $\kappa = 0$, then s is given by

$$s(\mathbf{r}) = \frac{1}{C_F}\frac{|\rho|}{\rho} = \frac{\lambda}{C_F}\rho^{-1/3} \tag{3.46}$$

As long as the electron density of an atom is described by Eq. 3.46 with different value of λ for each shell, then a step like diagram is represented by $s(\mathbf{r})$. Core,Valence-Core and Valence regions may be distinguished in such representation. As example, lets take a look to three closed-shell systems as He, Ne and Ar atoms. Placed the atoms at $\mathbf{r} = \mathbf{0}$, (Fig. 3.1, left column), one, two and three minima are obtained for He, Ne and Ar respectively in the $s(\mathbf{r})$ plot, splitting the space in three regions:

- **Pure core region**: From $\mathbf{r} = \mathbf{0}$ to the outermost maximum of $s(\mathbf{r})$.
- **Core-Valence(CV) transition region**: From the end of the core region to outermost minimum.
- **Pure valence region**: From the outermost minimum to the rest of space. Zupan et al [24], limits this region to include those contributions from the outermost shell whose reduced density gradients are comparable to those in the core. They defined a fourth tail region which covers the rest of space.

In this work we shall focus on the dependence of s with the electon density, ρ. From the $s(\rho)$ plots (Figs 3.1, right column) of He, Ne and Ar, comes that this representation do not solve atomic shell structure as well as $s(\mathbf{r})$. One and two minina are observed for He and Ne (the high density mininum of the K-L transition is only shown in the He plot, but it exists in the three cases), but there is no a third mininum for Ar as it should be expected. The missing of M shell is a consequence of the d orbitals. Keeping in mind the expression of $s(\rho)$ for a exponential density $s(\rho) = \lambda\rho^{-1/3}$, the factor $1/\rho$ prevents to split $s(\rho)$ in orbital contributions. Nevertheless, the orbitals with the same principal quantum number exhibit the main contribution to the total density at nearly the same distance from the nucleus. Thus, orbitals within a particular shell are predominant in the sum of densities being possible to split $s(\rho)$ in shell contributions. The changes in λ indicate the transition from one shell to another. However, if the density of one shell decreases significantly, before the density of the next shell reaches its maximum, the change in λ are overwhelmed by the increase of the term $1/\rho$, being worse as the distance of the shells increase. Figs 3.1 show a well resolved K, L shells, but a hardly defined outer M shell. Regarding their topology, $s(\mathbf{r})$ and $s(\rho)$ representations attain their minima values ($s = 0$) at CPs of $\rho(\mathbf{r})$. The number and the position of their CPs are exactly the same, and the density at such points are exactly the same. This equivalence may be easily probed by the chain rule:

$$\frac{ds(\rho)}{d\rho} = \frac{ds(\rho)}{d\mathbf{r}}\frac{d\mathbf{r}}{d\rho} = \frac{\frac{ds(\mathbf{r})}{d\mathbf{r}}}{\nabla\rho} \tag{3.47}$$

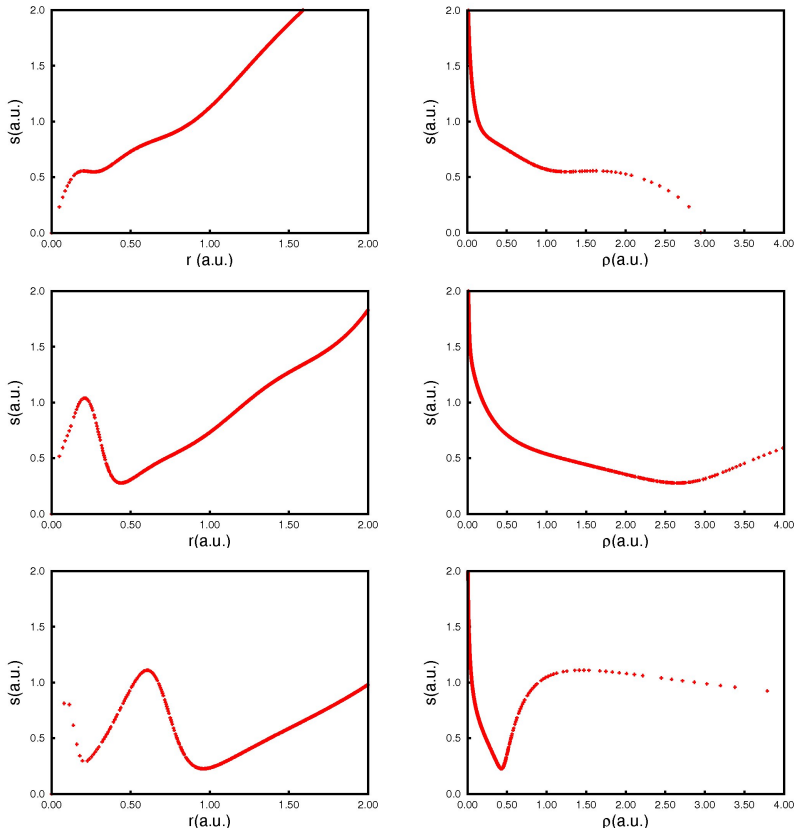

Table 3.1: Reduced density gradient for the He (top), Ne (middle) and Ar (bottom) atoms. s versus $\mathbf{r}$ is plotted in the left column and s versus ρ in the right column.

The zeros in the numerator are CPs of $s(\mathbf{r})$ and makes the above equation to satisfy the condition of CP for $s(\rho)$. The minima at CPs of ρ are consequence of the absolute value of the gradient of ρ in the numerator. As a matter of fact $s(\rho)$ is not differentiable at such positions.

3.3.2 Revealing NonCovalent Interactions

The analysis of chemical bonding by means of $s(\mathbf{r})$, reveals the capability of the reduced density gradient to differentiate between different kind of interactions. In particular, the properties of $s(\mathbf{r})$ has been widely exploit to define one the most successful descriptor of non-covalent interactions, the NCI index. From Eq 3.46, graphs of s versus ρ assume the form $s(\rho) = \frac{\lambda}{C_F}\rho^{-1/3}$. However, when any interaction occurs, the exponential density model is no longer valid, leading a peak in the diagram which may lead to a zero of $s(\rho)$ or not. In the former case, the interaction occurs through a BCP of $\rho(\mathbf{r})$, then NCI and AIM theory coincide. In the later, AIM is blind to the interaction, but no NCI. This is the case of steric hindrance, widely employed in Organic Chemistry to explain many

reaction mechanisms.

Once the different interactions have been localized, it is customary to differentiate between interaction types. The properties of the laplacian of the density ($\nabla^2\rho$) have been widely employed to classify chemical interactions[25]. The sign of $\nabla^2\rho$ indicates whether there is a concentration ($\nabla^2\rho < 0$) or a depletion ($\nabla^2\rho > 0$) of the charge density in a given region. The AIM classification of interaction is based on the sign of ($\nabla^2\rho$) at BCPs. Denoting as closed-shell interactions those with ($\nabla^2\rho > 0$) and shared interactions otherwise. Long range interactions are classified as closed-shell interaction with the AIM criteria, not being possible to differentiate them. Instead of using the laplacian of ρ, we can consider the accumulation or depletion of density in the plane perpendicular to the interaction. ($\nabla^2\rho$) is given by the sum of the three curvatures of ρ, $\lambda_1, \lambda_2, \lambda_3$. The last one represents the variation along the internuclear direction and is the dominant contribution to the laplacian , while λ_1, λ_2 represent variation in the plane normal to λ_3. Bonding interactions can be identified by the negative sign of λ_2, as for the hydrogen bonds and van der Waals interaction, whereas if atoms are in nonbonded contact $\lambda_2 > 0$, as in the case of steric hindrance.

Replacing the plots of $s(\rho)$ by plotting sign$(\lambda_2)\rho$ as the ordinate, the interaction types may be distinguished.

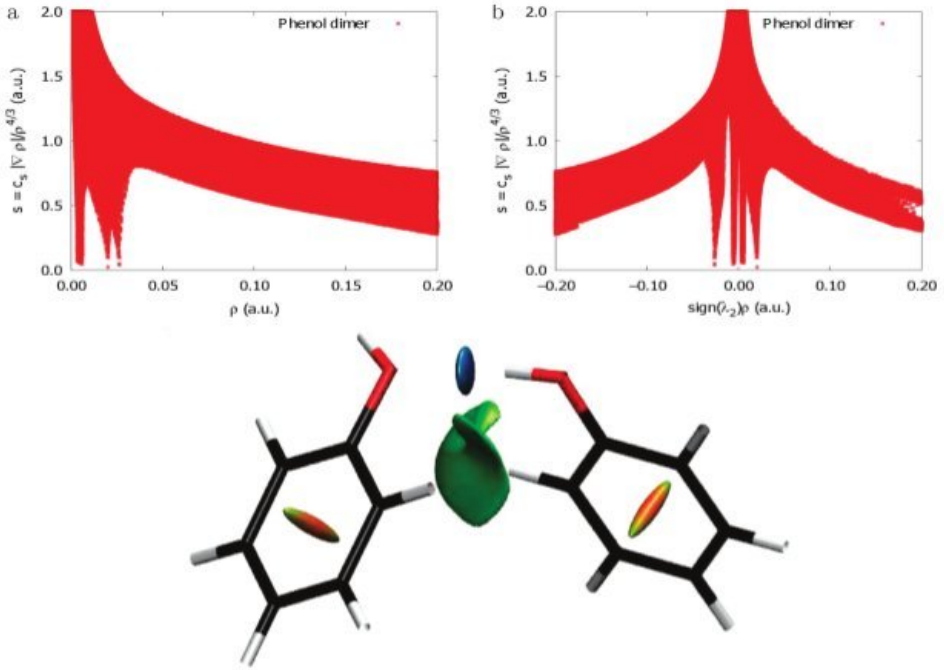

Figure 3.1: Plots of (a) $s(\rho)$, (b) sign$(\lambda_2)\rho$, and (bottom) NCI isosurface for phenol dimer. Blue indicates strong attraction, green indicates very weak interactions, and red indicates strong repulsion.

For example, the phenol dimer (Fig. 3.1) is a hydrogen-bonded complex, that also exhibits nonbonding interactions with each benzene ring. The hydrogen bonds are plo-

tted in the left part of diagram $s(\rho)$, at negative curvatures. By contrast, nonbonding interactions are plotted at the right part. Weak dispersion interactions between phenol rings appear as peaks near zero. The NCI isosurfaces are coloured according the nature of the interaction: blue for strong attractions, green for weak interactions and red for strong repulsions.

Although NCI index is mainly applied to systems governed by long range interactions, it has been found that ionic interactions may be successfully studied by NCI [26]

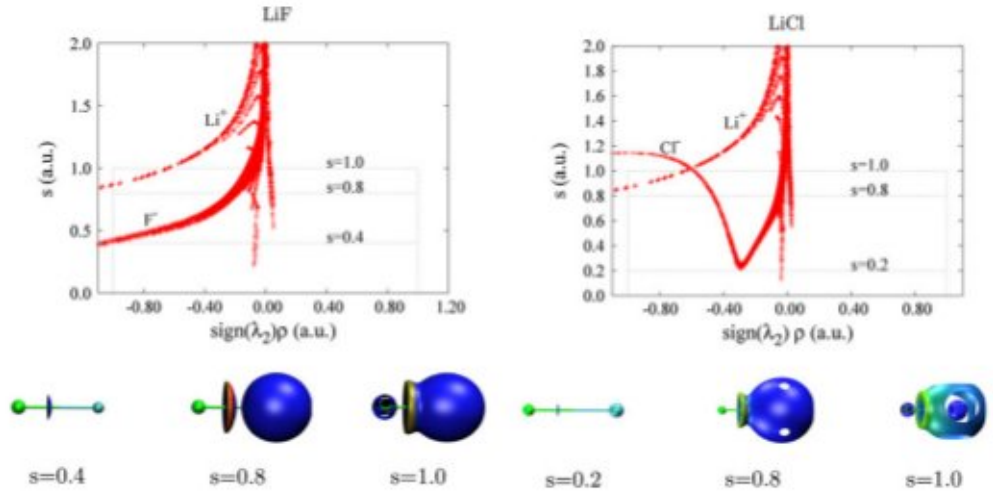

Figure 3.2: NCI for LiF(left) and LiCl(right). Top: $s(\rho)$), bottom: NCI isosurfaces for various cutoffs (indicates below each figure). The part of the $s(\rho)$ diagram covered by each isosurface is highlighted in $s(\rho)$ plot by the corresponding frames.

The $s(\rho)$ diagram for an ionic pair AB show two different decaying curves. This behavior may be explained in terms of promolecular densities models. As density in ionic crystals is fairly well described by promolecular densities [27], the density of an ionic pair at distance R may be modelled as

$$\rho(r) = \rho_A^{prom} + \rho_B^{prom} = ae^{-\alpha r} + be^{\beta(R-r)} \tag{3.48}$$

where (a, α) and (b,β) are positive constants characteristics of A and B ions, respectively. As $r \to r_A$, $\rho(r)$ may be approach as ρ_A. Then, the reduced density gradient reduces to free-ion behavior:

$$s(r \to r_A) = \alpha\rho^{-1/3} \tag{3.49}$$

These regions give rise to two curves of behavior $y = cx^{-1/3}$, being c the displacement of the curve along the y axis. The constants α and β are associated with the difficulty to deform, or hardness, of the ions [28]. The change in the slope at medium density observed in Fig. 3.2 are associated with changes from one shell to another. In the Chapter 6, we shall explore different covalent bonds by means the reduced density gradient.

4 Results

4.1 Examples and Computational Details

A bonding analysis based on reduced density matrices and NCI index of several test cases were carried out. These included closed-shell molecular systems in their electronic ground state and two open-shell molecules, B_2 and O_2 in their $^3\Sigma_u^+$ and $^3\Sigma_g^-$ ground states. The closed-shell systems are the homonuclear diatomic molecules A_2(A=H,He,Li, Be,B,C,N,O,F,Ne) and the heteronuclear molecules LiH and the H_2O. Additionally a comparative bonding analysis based on the NCI index was applied to different arrangements of octylamine in gas phase.

Aside from octylamine, all the calculations have used the *gamess* code to obtain the wave functions at Hartree-Fock level and different complete active space multiconfiguration calculations (CAS[n,m], n active electrons and m active orbitals: CAS[2,2] for H_2, CAS[4,4] for He_2, CAS[4,4] for Li_2, CAS[4,4] for Be_2, CAS[6,8] for B_2, CAS[8,8] for C_2, CAS[10,8] for N_2, CAS[12,10] for O_2, CAS[14,8] for F_2, CAS[16,14] for Ne_2, CAS[2,2] for LiH and CAS[6,10] for the H_2O. The standard 6-311G(d,p)++ basis set were used. A QTAIM real space partition was chosen. The analysis of the wave function was performed with the *promolden* code. The numerical integrations in *promolden* used β-spheres. Inside the spheres 1000 points Gauss-Chebychev second kind radial quadrature and a Lebedev angular quadrature with 200 points were used, considering generalized energy multipoles up to L=4. Outside the spheres a trapezoidal radial quadrature with 800 points and a 6000 angular points Lebedev quadrature were used with generalized energy mulitipoles up to L=8. All the calculations were performed at the CASSCF equilibrium geometry. The energies and the electron densities for the arrays of octylamine were calculated at DFT level, with the rPBE [29]functional including Grimme D2 [30] approach as implemented in the VASP code [31]. Projector Augmented Wave Pseudopotentails combined to plane waves (cutoff=400ev) represent the electronic distribution.

Reduced density matrices and cumulants needed to performed the NAdOs analysis has been obtained with the code *DENMAT*. The NCI analysis were accomplished with *NCIPLOT* [32], and *critic2* [33] codes

4.1.1 Illustrative Results

Homonuclear Molecules

Tables 4.1 to 4.10 contain $\langle N_{ab} \rangle$ and $\langle N_{aa} \rangle$ of all the diatomic molecules analysed at RHF and CASSCF theory levels. It is easy to notice how chemical bonding may be split into σ and π elements . All the homonuclear molecules examined suffer a decrease of

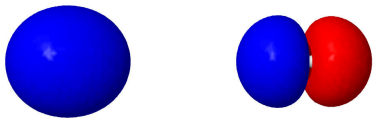

0.411 0.005

Figure 4.1: Two-center NAdOs for the H_2 molecule.

their delocalization indices, $\delta_{ab} = 2\langle Nab\rangle$, at correlated level. A deep inspection of the eigenvalues of each NAdO reveals how correlation acts over chemical bonding. By one hand, there is a reduction of the eigenvalues of the σ and π NAdOs. On the other hand , negative eigenvalues are assigned to the NAdOs that emerge from the virtual orbitals at RHF level.

n_i^{ab}	RHF	CAS	$\langle N_{ab}\rangle$	RHF	CAS
n_1^{ab}	0.5000	0.4114	$\langle N_{ab}\rangle$	0.4999	0.4164
n_2^{ab}		0.0049	$\langle N_{aa}\rangle$	0.4999	0.5835
			$\langle N_a\rangle$	0.9999	1.0002

Table 4.1: Two-center eigenvalues (n_i^{ab})and $\langle N_{ab}\rangle$ population for the H_2 molecule.

Let us start with H_2. At RHF level, the wave function is formed by one symmetric MO, $1\sigma_g$. Consequently, the diagonalization of the D_{HH} matrix leads to one NAdOS of the same symmetry with an eigenvalue of 0.5. At CAS[2,2] level the wave function is build from $1\sigma_g$ and $1\sigma_u$ orbitals, leading to one symmetric and one antisymmetric NAdOs respectively. The former recovers the 98.7% of the delocalization index. Thus, the single bond picture of H_2 bond is given by the $1\sigma_g$ orbital.

Opposite to H_2, the bonding in the He_2 has been classified as a closed-shell interaction, giving a delocalization index of only 0.002 at RHF and at CASSCF level. The orbital picture recovered by the NAdOs resemble us to two noninteracting He atoms. The single-determinant wave function is not able to describe closed-shell interactions. Including correlation by means σ orbitals hardly improves the bond descriptions, being necessary to introduce π components in the wave function.

All the others molecules analysed are formed by elements with two atomic shells, K and L, and consequently with a core-valence separation. The first two NAdOs of all the systems analysed emerged form the combination of core MOs $1\sigma_g$ and $1\sigma_u$, yielding a negligible contribution to the bonding and thus leading a core-valence NAdOS separation. In what follows we are going to focus only in the valence NAdOs.

The first chemically meaningful contribution to the Li-Li bonding is the NAdO 3, recovering by itself almost 99.9 % of δ^{LiLi} at RHF level. Although correlation also

n_i^{ab}	RHF	CAS	$\langle N_{ab} \rangle$	RHF	CAS
n_1^{ab}	0.0005	0.0006	$\langle N_{ab} \rangle$	1.9998	1.9987
n_2^{ab}	0.0005	0.0006	$\langle N_{aa} \rangle$	0.0010	0.0012
n_3^{ab}		-0.000	$\langle N_a \rangle$	1.9999	1.9999
n_4^{ab}		-0.000			

Table 4.2: Two-center eigenvalues (n_i^{ab})and $\langle N_{ab} \rangle$ population for the He_2 molecule.

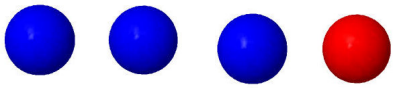

RHF: 0.0005 0.0005
CAS: 0.0006 0.0006

Figure 4.2: Two-center NAdOs for the He_2 molecule.

reduced, n_3^{ab}, the change is not so dramatic as in the H_2 molecule (0.5000 $\rightarrow$ 0.4114 in H_2, and 0.5000 $\rightarrow$ 0.4114),

n_i^{ab}	RHF	CAS	$\langle N_{ab} \rangle$	RHF	CAS
n_1^{ab}	0.0000	0.0000	$\langle N_{ab} \rangle$	0.4977	0.3139
n_2^{ab}	0.0000	0.0000	$\langle N_{aa} \rangle$	2.4977	2.6804
n_3^{ab}	0.4977	0.4800	$\langle N_a \rangle$	2.9955	2.9943
n_4^{ab}		0.0163			

Table 4.3: Two-center eigenvalues (n_i^{ab})and $\langle N_{ab} \rangle$ population for the Li_2 molecule.

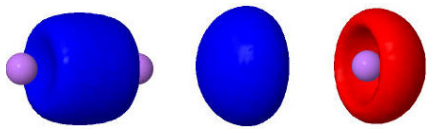

RHF: 0.4977
CAS: 0.4800 0.0163

Figure 4.3: Two-center NAdOs for the Li_2 molecule.

Similarly to He_2, the bonding in Be_2 is a closed-shell interaction. The combination of the $2s$ orbitals recovers almost 99.9% of δ^{BeBe}. Including the $2p_z$ combinations, leads to NAdOs with negative contribution, being the sum of 2σ orbitals greater than δ^{BeBe}.

B_2 is the first open-shell system of the set. Its ground electronic configuration at ROHF level presents two single occupied π MO, while all the others MO remain doubly

n_i^{ab}	RHF	CAS	$\langle N_{ab} \rangle$	RHF	CAS
n_1^{ab}	0.0000	0.0000	$\langle N_{ab} \rangle$	0.0082	0.0075
n_2^{ab}	0.0000	0.0000	$\langle N_{aa} \rangle$	3.9900	3.9912
n_3^{ab}	0.0040	0.0039	$\langle N_a \rangle$	3.9983	3.9912
n_4^{ab}	0.0042	0.0039			
n_5^{ab}		-0.0001			
n_6^{ab}		-0.0001			

Table 4.4: Two-center eigenvalues (n_i^{ab})and $\langle N_{ab} \rangle$ population for the Be_2 molecule.

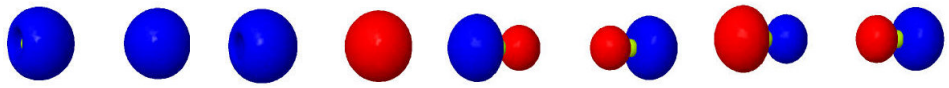

RHF:	0.0040	0.0042		
CAS:	0.0039	0.0039	-0.0001	-0.0001

Figure 4.4: Two-center NAdOs for the Be_2 molecule.

occupied. The π elements rise the bond order to two. The asymmetry in the σ-π population leads to π NAdOs with lightly lower eigenvalues than σ. At CASSCF level there is a complete $\sigma - \pi$ separation, depleting the π_g elements and rising the σ_g NAdOs. The symmetry respect to the inversion center seems to be also differentiate at correlated level, breaking the quasidegenaracy of NAdOS 3 and 4. The orbitals 7, 8, 9 and 10 come from the RHF virtual orbitals, and all of them posses negative eigenvalues. The double bond found at ROHF level, changes to a single bond picture governed by the σ contributions at CASSCF level.

Adding two electrons to the $2\pi_g$ of B_2, leads to the closed-shell configuration of C_2. At RHF, the σ component plays almost the same role in both systems, but the π NAdOs contribution rises the C-C bond order to 3.18 . Correlation effects are quite

n_i^{ab}	ROHF	CAS	n_i^{ab}	CAS	$\langle N_{ab} \rangle$	ROHF	CAS
n_1^{ab}	0.0000	0.0000	n_9^{ab}	-0.0007	$\langle N_{aa} \rangle$	3.9652	4.3357
n_2^{ab}	0.0000	0.0000	n_{10}^{ab}	-0.0010	$\langle N_{ab} \rangle$	1.0344	0.6648
n_3^{ab}	0.2672	0.2995			$\langle N_a \rangle$	4.9997	5.0005
n_4^{ab}	0.2672	0.0199					
n_5^{ab}	0.2499	0.1601					
n_6^{ab}	0.2499	0.1601					
n_7^{ab}		-0.0440					
n_8^{ab}		-0.0007					

Table 4.5: Two-center eigenvalues (n_i^{ab})and $\langle N_{ab} \rangle$ population for the B_2 molecule.

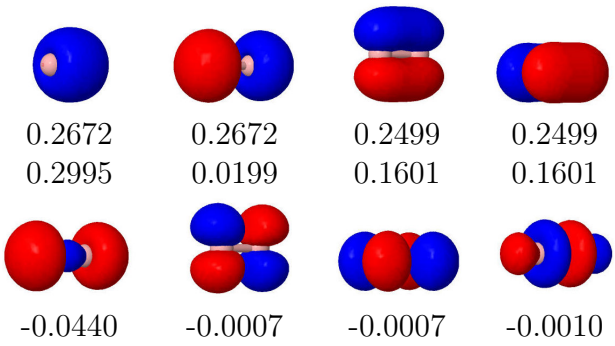

Figure 4.5: Two-center NAdOs for the B_2 molecule.

n_i^{ab}	RHF	CAS	n_i^{ab}	CAS	$\langle N_{ab} \rangle$	RHF	CAS
n_1^{ab}	0.0000	0.0000	n_9^{ab}	-0.0121	$\langle N_{aa} \rangle$	4.4060	5.1094
n_2^{ab}	0.0000	0.0000	n_{10}^{ab}	-0.0121	$\langle N_{ab} \rangle$	1.5941	0.8908
n_3^{ab}	0.2970	0.3375			$\langle N_a \rangle$	6.0002	6.0002
n_4^{ab}	0.2970	0.0830					
n_5^{ab}	0.5000	0.2696					
n_6^{ab}	0.5000	0.2696					
n_7^{ab}		-0.0427					
n_8^{ab}		-0.0021					

Table 4.6: Two-center eigenvalues (n_i^{ab})and $\langle N_{ab} \rangle$ population for the C_2 molecule.

similar in both systems, differentiating between σ and π orbitals and between *gerade* and *ungerade*. Again, the virtual RHF orbitals lead to NAdOs with negative eigenvalue.

The triple bond of N_2 at RHF level is clearly described in terms of two π and one σ bonds. Contrary to C_2 and B_2, the σ component is governed by the $3\sigma_g$ orbital, instead of $2\sigma_g$ and $2\sigma_u$. Once again, the correlation breaks the equilibrium between orbitals 6,4 and 5, differentiating again σ and π components. 6 and 7 eigenvalues changes from 0.50 to 0.29, while the NAdO 5 form 0.5 to 0.38. As in the previous case, all the virtual orbitals have negative contributions.

Similarly to B_2, O_2 ground state is a triplet, with a bond order above 2 at single determinant level. However, the picture is more complex, than in the previous case, leading a main σ contribution and leaving the π_g contribution in the background. There is a non negligible contribution of π_u NAdOs 8 and 9. Contrary to what we have found in other molecules, there is an important role of NAdO 10, introduced at correlated level.

F-F bond is by far the most challenging system of the set. Long is the story of this molecule, widely studied by old VB and MO theories and by the most modern AIM theory and ELF approaches. Sason Shaik and co-workers has labelled the F-F bond as

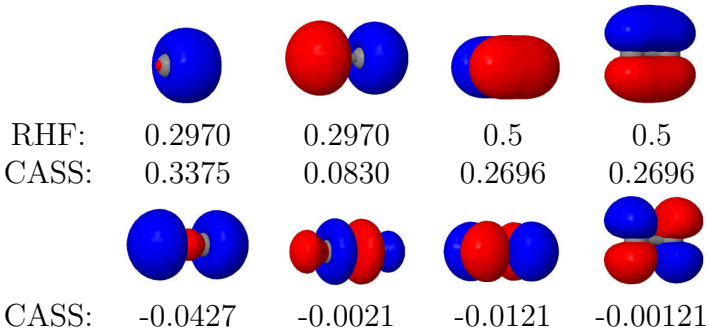

Figure 4.6: Two-center NAdOs for the C_2 molecule.

n_i^{ab}	RHF	CAS	n_i^{ab}	CAS	$\langle N_{ab} \rangle$	RHF	CAS
n_1^{ab}	0.0000	0.0000	n_9^{ab}	-0.0154	$\langle N_{aa} \rangle$	5.4802	6.0319
n_2^{ab}	0.0000	0.0000	n_{10}^{ab}	-0.0152	$\langle N_{ab} \rangle$	1.5197	0.9678
n_3^{ab}	0.5000	0.0120			$\langle N_a \rangle$	6.9999	6.999
n_4^{ab}	0.0098	0.0228					
n_5^{ab}	0.0098	0.3880					
n_6^{ab}	0.5000	0.2954					
n_7^{ab}	0.5000	0.2954					
n_8^{ab}		-0.0154					

Table 4.7: Two-center eigenvalues (n_i^{ab})and $\langle N_{ab} \rangle$ population for the N_2 molecule.

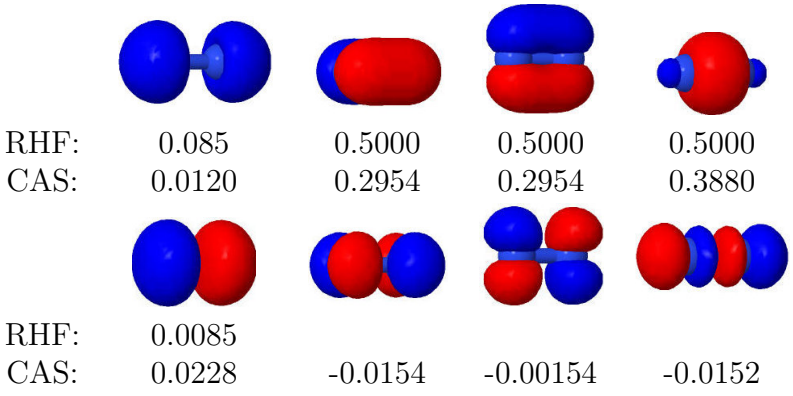

Figure 4.7: Two-center NAdOs for the N_2 molecule.

charge-shift bonding [34]. They claimed that the covalent-ionic fluctuation is the source of the bonding. Turning out to NAdO analysis we found that only the NAdO σ 5 rules the interaction between F atoms at HF and correlated level. The dramatic change of n_8^{ab} from positive to negative value (0.0093(RHF) $\rightarrow$ -0.0106(CAS)) may be connected with the special features of the system. More work should be devoted to rationalize negative

n_i^{ab}	ROHF	CAS	n_i^{ab}	CAS	$\langle N_{ab} \rangle$	ROHF	CAS
n_1^{ab}	0.0000	-0.0000	n_{11}^{ab}	-0.0079	$\langle N_{aa} \rangle$	6.8843	7.2302
n_2^{ab}	0.0000	-0.0000	n_{12}^{ab}	-0.0022	$\langle N_{ab} \rangle$	1.1155	0.7698
n_3^{ab}	0.0010	0.2451			$\langle N_a \rangle$	7.9999	7.9999
n_4^{ab}	0.0010	0.0540					
n_5^{ab}	0.5000	0.1160					
n_6^{ab}	0.2738	0.1160					
n_7^{ab}	0.2738	0.0104					
n_8^{ab}	0.0238	0.0104					
n_9^{ab}	0.0238	0.0051					
n_{10}^{ab}		0.2222					

Table 4.8: Two-center eigenvalues (n_i^{ab})and $\langle N_{ab} \rangle$ population for the O_2 molecule.

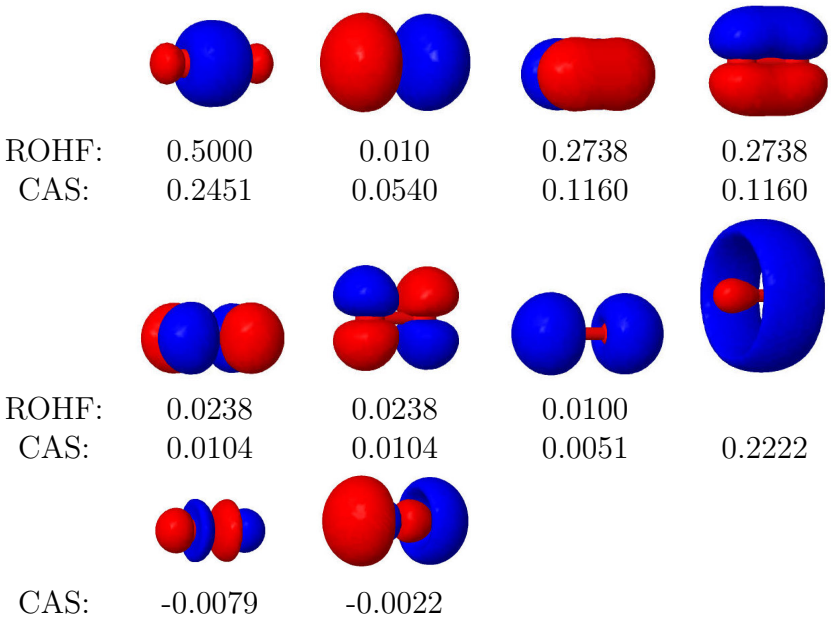

Figure 4.8: Two-center NAdOs for the O_2 molecule.

eigenvalues.

The picture recovered by Ne_2 is quite similar to those obtained for the previous closed-shell interactions examined. Only combinations of atomic orbitals s, p_z, d_{z^2} and z components in general (internuclear axis are fixed along z direction) are relevant to the interaction. Contrary to the previous system, $\langle N_{ab} \rangle$ increases with the correlation and consequently, NAdOs 5 and 10, extended along z axis slightly increase its eigenvalues.

Additionally a NCI analysis was also carried out to the same set of molecules at correlated level. Let us start with the set H_2, Be_2 and N_2 as examples of covalent and dispersion bonding.

n_i^{ab}	RHF	CAS	n_i^{ab}	CAS	$\langle N_{ab} \rangle$	RHF	CAS
n_1^{ab}	0.0000	-0.0000	n_{11}^{ab}	-0.0108	$\langle N_{ab} \rangle$	0.5543	0.4249
n_2^{ab}	0.0000	0.0000	n_{12}^{ab}	0.0056	$\langle N_{aa} \rangle$	8.3435	8.5750
n_3^{ab}	0.0046	0.0244			$\langle N_a \rangle$	8.8978	8.9999
n_4^{ab}	0.0093	0.0244					
n_5^{ab}	0.0135	0.0243					
n_6^{ab}	0.0135	0.0243					
n_7^{ab}	0.4700	0.0214					
n_8^{ab}	0.0216	-0.0106					
n_9^{ab}	0.0216	0.2902					
n_{10}^{ab}		0.0314					

Table 4.9: Two-center eigenvalues (n_i^{ab})and $\langle N_{ab} \rangle$ population for the F_2 molecule.

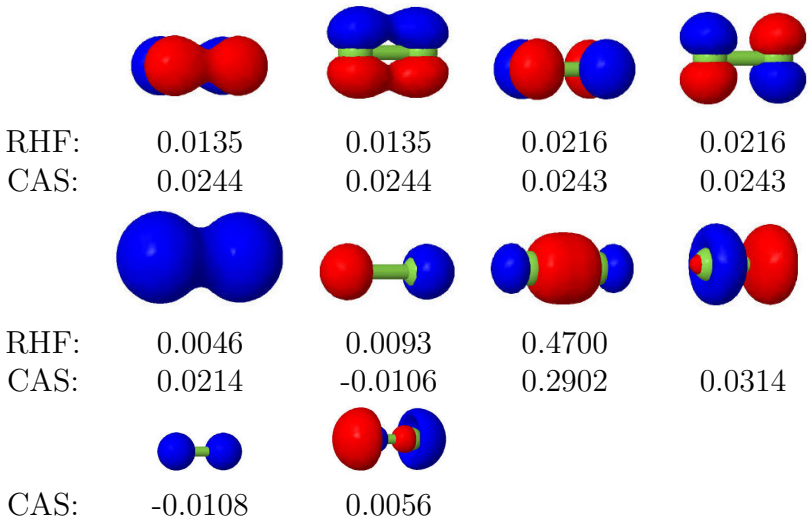

Figure 4.9: Two-center NAdOs for the F_2 molecule.

As it was mentioned in the theoretical part, the main features of $s(\rho)$ are the zeros at electron density CPs, and this is what is obtained for the H_2 molecule (Fig. 4.11). The isosurface of $s(\mathbf{r})$ is completely delocalized along the H_2 bond. As observed in hydrogen bonds[35], there is a peak at positive curvatures induced by the density overlap.

Aside from the zero at BCP and at nuclear positions, $s(\rho)$ for Be_2(Fig. 4.12) has a critical point at higher density than the BCP. A deeply analysis of the reduced density gradient for the Be atom, makes clear that this CP is related with the change from one atomic shell to another. At low densities $s(\mathbf{r})$ is dominated by the K shell, where at higher is the L shell the dominant. The $s(\mathbf{r})$ isosurface may be split in two regions with negative curvature around the Be nuclei and a disc-shaped surface around the BCP with low curvature. From this picture, the Be_2 may be then envisioned as a weak interaction

n_i^{ab}	RHF	CAS	n_i^{ab}	CAS	$\langle N_{ab...} \rangle$	RHF	CAS
n_5^{ab}	0.0011	0.0015	n_{14}^{ab}	-0.0001	$\langle N_{aa} \rangle$	9.9972	9.9962
n_6^{ab}	0.0000	0.0003	n_{15}^{ab}	-0.0001	$\langle N_{ab} \rangle$	0.0027	0.0037
n_7^{ab}	0.0000	0.0003			$\langle N_a \rangle$	10.000	10.0000
n_8^{ab}	0.0000	0.0003					
n_9^{ab}	0.0000	0.0003					
n_{10}^{ab}	0.0011	0.0015					
n_{12}^{ab}		-0.0001					
n_{13}^{ab}		-0.0001					

Table 4.10: Two-center eigenvalues (n_i^{ab})and $\langle N_{ab} \rangle$ population for the Ne_2 molecule.

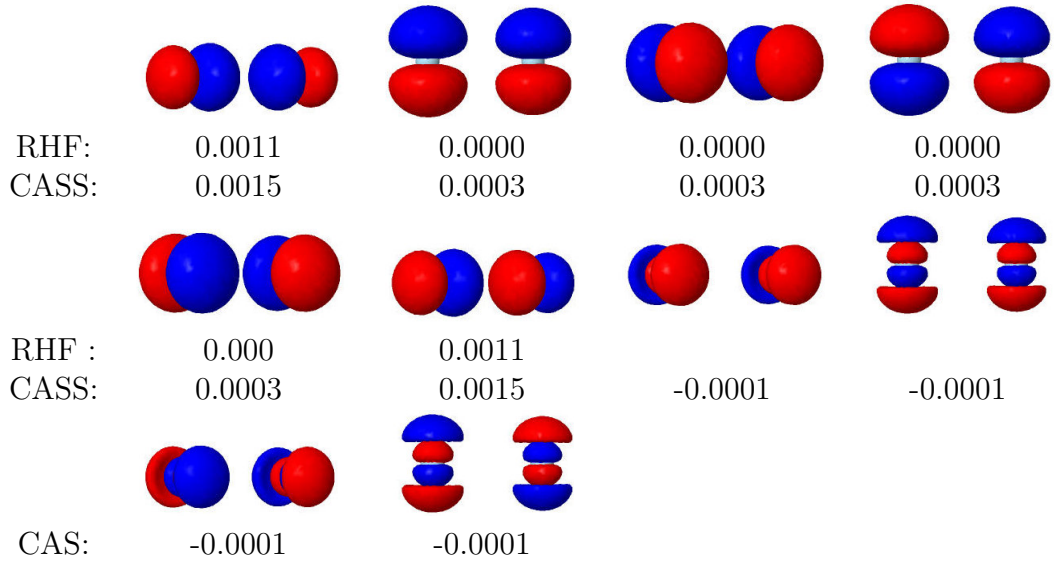

Figure 4.10: Two-center NAdOs for the Ne_2 molecule.

between two Be atoms placed far away from each other.

As a prototype of multiple bonding let us consider the N_2 molecule (Fig. 4.11). $s(\mathbf{r})$ is quite similar to the H_2 , as it is expected for a covalent interaction. The transition from the K shell to the L atomic shell of N is reproduce at high densities. he higher values of ρ at the nuclear positions, makes that at $s(\mathbf{r})$=0.5, the isosurface encloses the whole molecule.

These three examples clarify how the reduced density gradient can differentiate between shared-sell interactions (H_2 and N_2) and closed-shell interactions (Be_2). The former gives isosurfaces extended along the bond, with a peak at positive curvatures enclosing the BCP of $\rho(\mathbf{r})$. The later lead to disc-shaped isosurfaces , around the BCP, with near zero curvatures. By contrast $s(\mathbf{r})$ may not be factorized in orbital components, only being possible to differentiate shared-shell interactions from local analysis of the

electron density at BCPs. Combining the features observed by the above examples, it is possible to rationalize the behavior of $s(\mathbf{r})$ for the rest of the set.

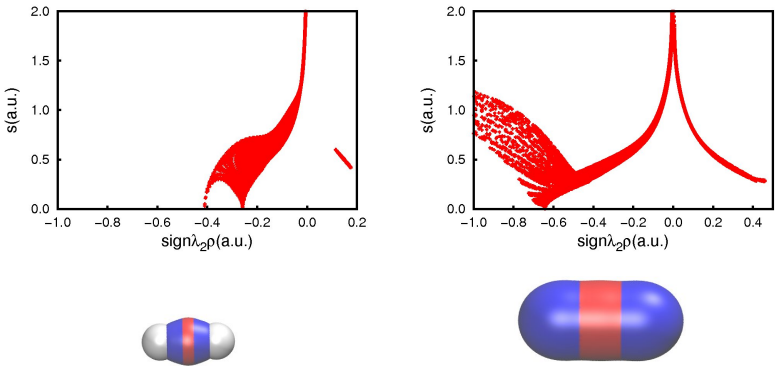

Figure 4.11: s(ρ) plots and NCI isosurface of H_2 (left) and N_2(right). Isosurfaces were generated at s=0.5 a.u.

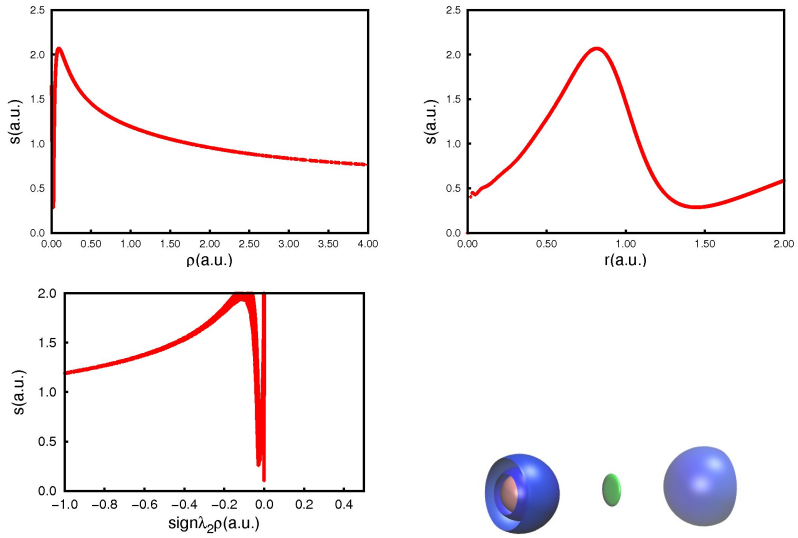

Figure 4.12: Top: s(ρ) and s($\mathbf{r}$) plots of Be. Bottom: s(ρ) plots and NCI isosurface (s=0.5 a.u.) of Be_2 .

Non nuclear maximum of Li_2 [36],[37], yields a $s(\mathbf{r})$ isosurface completely different from the above systems(Fig. 4.11). The overlap between densities is much weaker, yielding a peak at positive curvature close to zero. B_2 and C_2 looks similar to N_2, not being possible to distinguish the different bond orders. He_2 and Ne_2 recover the same closed-shell picture as Be_2, as it is expected.

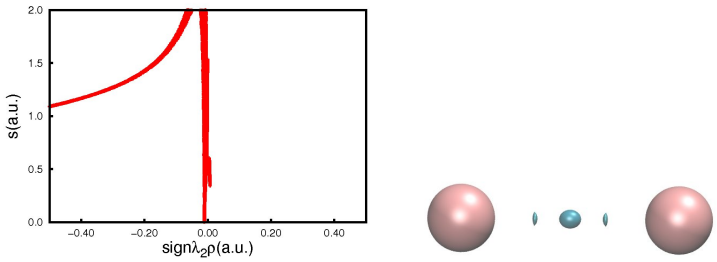

Table 4.11: s(ρ) plots and NCI isosurface (s=0.05 a.u.) of Li_2

The bonding in the O_2 and in the F_2, merges many properties of of the N_2 and the closed-shell interaction of Be_2. The charge-shift character of this two bonds may then be easily grasped by NCI. As reported in the work of Shaik [34],[38] the sum of electronegatives is closely related with the charge-shift character, increasing form the C_2 to the F_2, following the same trends as the bumps of the $s(\mathbf{r})$ isosurface. The additional CPs of $s(\rho)$ give rise to a more remarkable atomic character than N_2. The absence of such CPs in He_2, Li_2, B_2, C_2 and N_2 may be rationalized as a non-neglible missing of the valence atomic shell (K for He, and L for the others).

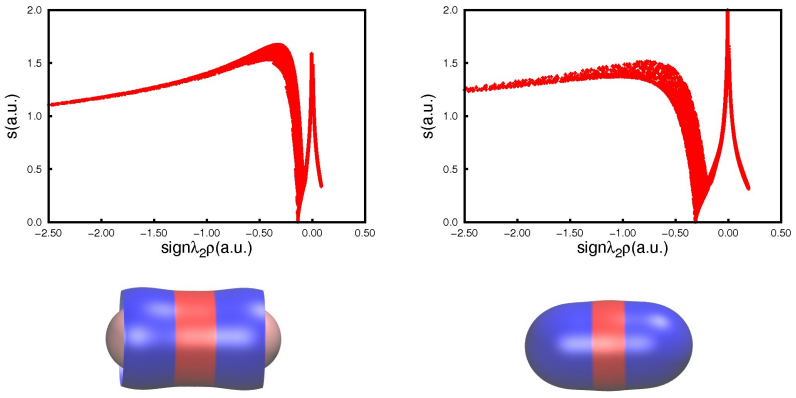

Figure 4.13: s(ρ) plots and NCI isosurface (s=0.5 a.u.) of B_2 (left) and C_2(right)

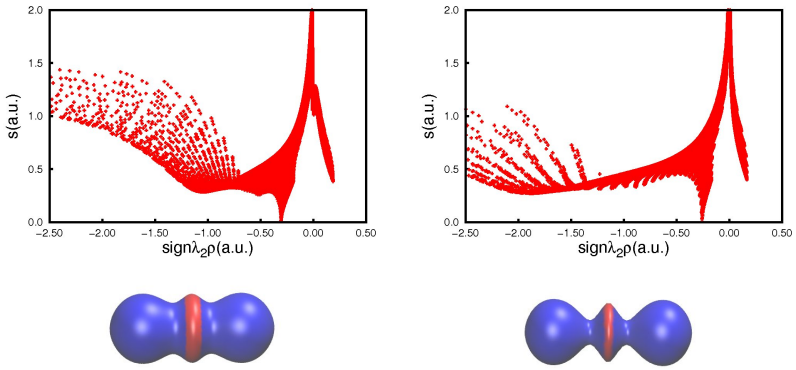

Table 4.12: s(ρ) plots and NCI isosurface (s=0.5 a.u.) of O_2 (left) and F_2(right)

Heteronuclear Molecules

Leaving homonuclear molecules, the change induced by the polarity in the bonding were also analysed. LiH and H_2O (Tables 4.13 and 4.14) were examined as example of ionic and covalent compounds respectively. As is expected, the delocalization indices decrease in order H_2O ,LiH. $\langle$ N_{ab} $\rangle$ in the two examples is almost recovered by only one eigenvalue, 94%, 98% and 93% and 94% in the RHF(CAS) calculation of LiH and H2O respectively, confirming that, Li-H and O-H bonds are single two-center, two-single (2c,2e) bonds [13]. (Figs 4.16). Regarding the effects of the correlation, different trends are observed depending on the nature of the interaction. As a close-shell interaction $\langle N_{LiH} \rangle$ increases, through a increase of $\langle N_{LiLi} \rangle$ and a decrease of $\langle N_{HH} \rangle$. By contrast, $\langle N_{OH} \rangle$ decreases in favour of $\langle N_{HH} \rangle$ and $\langle N_{OO} \rangle$.

n_i^{ab}	RHF	CAS	$\langle N_{ab} \rangle$	RHF	CAS
n_1^{ab}	0.0060	0.0060	$\langle N_{aa} \rangle$	1.9932	1.998
n_2^{ab}	0.098	0.1132	$\langle N_{bb} \rangle$	1.7945	1.7672
n_3^{ab}		-0.0038	$\langle N_{ab} \rangle$	0.1048	0.1155
			$\langle N_a \rangle$	2.0984	2.1139
			$\langle N_b \rangle$	1.8993	1.8828

Table 4.13: Two-center eigenvalues (n_i^{ab})and $\langle N_{ab} \rangle$ population for the LiH molecule. Labels a, b are for Li and H respectively

The NCI analysis also reveals a number of differences among two molecular systems. As it was explained in the Chapter4, and the ionic character of LiH, yields to two different curves in the $s(\rho)$ representation. Since Li cation is harder than the hydride, the Li^+ curve is over the hydride curve. The anionic behavior of the H may be grasped from the CP of the hydride curve, not present in the H_2 (Fig 4.11). By contrast, the covalent character of O-H bond, leads to a single curve. As the polarity of the bond decreases, the promolecular density model is no longer valid and, thus a single curve is

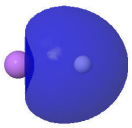

RHF: 0.098
CASS: 0.1132

Figure 4.14: Two-center NAdOs of the LiH molecule. The purple atom represents the Li, and the white the H.

n_i^{ab}	RHF	CAS	n_i^{ab}	CAS	$\langle N_{ab} \rangle$	RHF	CAS
n_1^{ab}	0.0000	0.0000	n_9^{ab}	0.0003	$\langle N_{aa} \rangle$	8.5434	8.5722
n_2^{ab}	0.0021	0.0081	n_{10}^{ab}	0.0006	$\langle N_{bb} \rangle$	0.0718	0.0980
n_3^{ab}	0.3046	0.0293	n_{11}^{ab}	-0.0000	$\langle N_{ab} \rangle$	0.3263	0.3020
n_4^{ab}	0.0075	0.0197			$\langle N_a \rangle$	8.8697	8.8742
n_5^{ab}	0.0120	0.2839			$\langle N_b \rangle$	0.3981	0.3101
n_6^{ab}		-0.0062					
n_7^{ab}		-0.0167					
n_8^{ab}		-0.0171					

Table 4.14: Two-center eigenvalues (n_i^{ab})and $\langle N_{ab} \rangle$ population for the H_2O molecule. Labels a and b are for O and H respectively.

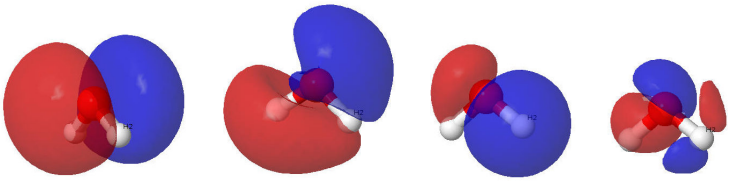

RHF: 0.0120 0.0075 0.3046
CASS: 0.0293 0.0197 0.2839 -0.0167

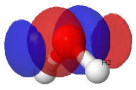

CASS: -0.0171

Figure 4.15: O-H NAdOs of the H_2O molecule.

observed. Similar to the O_2 (Fig 4.12), there is a remainder atomic shell structure of the oxygen.

The NCI isosurfaces place a disc-shaped isosurfaces appear between the Li and the H, encapsulating the H at higher values(Fig. 4.17). By contrast, H2O (Fig. 4.16) are delocalized along the O-H bond. Since the BCP is closer to the hydrogen atom, the

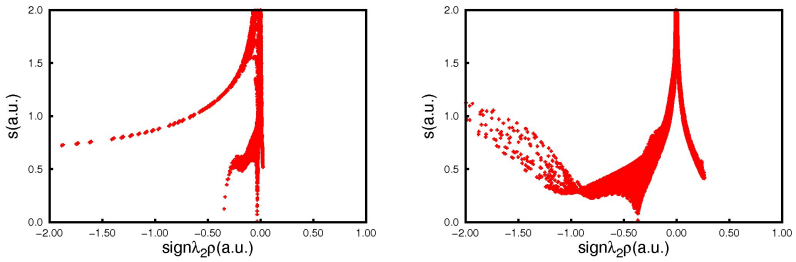

Figure 4.16: $s(\rho)$ of (left) LiH,(right) H_2O.

isosurfaces grow from it toward the lithium atom. Qualitatively the picture offered by NCI coincides with the shape of the main NAdO of O-H and Li-H bonds.

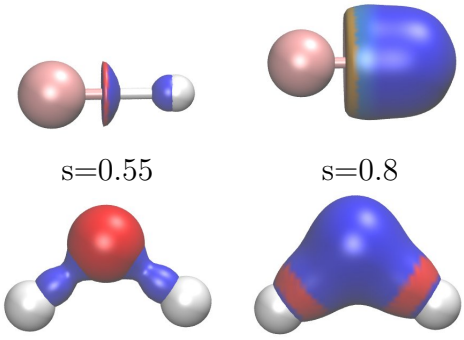

Figure 4.17: NCI isosurfaces for various cutoffs.(Top) LiH, (bottom) H_2O.

Long-range interactions

Once strong short-range interactions has been deeply investigated, we will focus in a weaker kind of interactions, already shown in He_2, Ne_2 , the so-called, noncovalent interactions. Many biological and extended systems, such as proteins, molecular solids, polymers ..., are stabilized through these long-range interactions. Although both bonding analysis above employed, NAdOs and NCI analysis, are perfectly valid to describe these interactions, the latter has been widely accepted by the community, whereas the application of the former to extended systems remains unexplored. To understand how NCI index reveals many insights of the noncovalent interactions in extended systems, we consider the prototypical example of octylamine self-assembly monolayers (SAMs). SAMs systems are formed by long alkyl molecules forming a two dimensions layer bind to a metallic surface. The stabilization of these system comes from the intermolecular interactions between the alkyl chains. To understand the nature of these interactions

we have compared the NCI isosurfaces of a 2 dimension polymer of octylamine with two linear polymers through different directions.

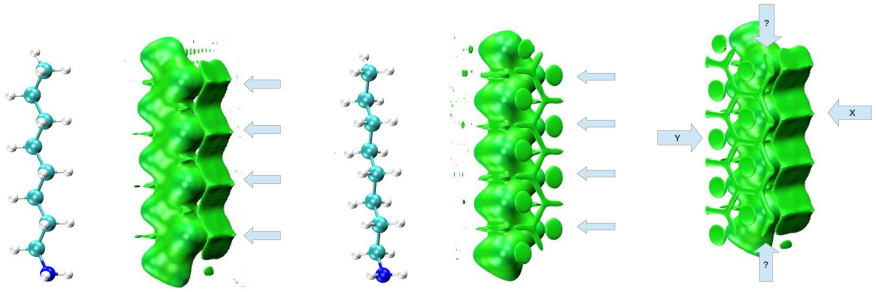

Figure 4.18: NCI isosurfaces of the x-polymer (left), the y-polymer (center) and the 2 dimension polymer. Only the monomers are plotted. The linear polymers grow in the plane. The interactions along different directions are labelled by arrows in the 2 dimension polymer. The additional interactions is labelled as ?.

The x-polymer shows a NCI isosurface completed delocalized along the chains(Fig 4.18). There are a direct interaction between the hydrogen atoms of different monomer in the y-polymers. This interaction leads to a round isosurfaces located between each pair of hydrogen atoms. Although many sistems with destabilizing H-H interaction were reported, these interactions makes the y-polymer more stable than the x-polymer (Fig 4.19). Aside of all these interactions, the 2 dimension polymer isosurface reveals an additional interactions giving rise to an hexagon-shape isosurfaces around each H-H interaction along y direction, which leads to its stabilization respect the linear polymers.

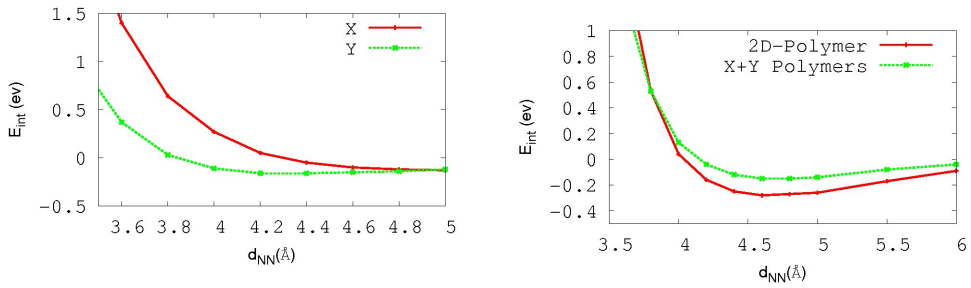

Figure 4.19: (Left) Interaction energies per monomer of octylamine (E_{int})for x and y polymers versus the distance between the chains (d_{NN}). (Right)(E_{int}) of the 2D polymers and the sum of the x and y polymers.

5 Conclusiones

El objetivo de esta memoria es explorar el enlace químico en el espacio real mediante dos técnicas de vanguardia que a día de hoy apenas han sido explotadas. Algunas de las conclusiones que se pueden extraer de este trabajo son:

1. Los índices de deslocalización resultan ser el principal nexo de unión entre los relativamente modernos análisis del enlace químico en el espacio real y los tradicionales órdenes de enlace definidos en un espacio orbital, permitiendo clasificar cuantitavamente los diferentes tipos de enlace. La partición de la densidad electrónica utilizando cuencas de Bader y la posterior factorización de dichas particiones, permiten recuperar el lenguaje orbital a partir de funciones definidas en el espacio real, como son los orbitales naturales adatativos. Los NAdOs permiten desglosar los índices de deslocalización en contribuciones monoelectrónicas, pudiendo racionalizar el enlace químico en términos de componentes π y σ , tan arraigados en el lenguaje de la química. A lo largo de este trabajo únicamente se han examinado los NAdOs precendentes de particiones de dos centros de la densidad electrónica, extender este análisis a particiones multicéntrica podría conducir a una mayor comprensión de algunos de los principales retos de la química teórica, como son la aromaticidad y el enlace multicéntrico.

2. El gradiente densidad de reducido permite caractérizar el enlace químico en terminos de interacciones de capa cerrada y capa abierta. Los multiples sistemas examinados a lo largo de esta memoria, así como otros muchos ya publicado, revelan la capacidad de s para diferenciar interacciones covalentes de interacciones de capa cerrada como son las enlaces iónicos o las débiles interacciones presentes en sistemas tales como He_2 o Be_2. La defínción de $s(\mathbf{r})$ imposibilita una descompsoción orbital similar a los NAdOs, conduciendo a una descripción superficial del enlace. Sin embargo, los análisis basados en el gradiente densidad, tales como NCI, son especialmente útiles para analizar interacciones débiles, en muchos casos no caracterizadas mediante análisis de otros campos escalares tales como la densidad electrónica o la ELF, y por lo tanto haciéndolo más apropiado para el estudio de estas interacciones presentes en muchos sistemas de interés biológico.

3. Mediante el análisis de los NAdOS y del gradiente densidad reducido, es posible abarcar todo tipo de enlace, desde las fuertes interacciones covalentes, hasta las débiles interacciones de dispersión. Una futura combinación de ambos métodos podría abrir las puertas a un análisis topológico del enlace en sistemas más realistas que los que se han tratado.

6 Appendix

Efficient computation of ρ_C^n's depends on simple algorithms to obtain their algebraic expressions. One of the most efficient starts by recalling that the r^{th} central moment ρ_r of a probability distribution function $f(x)$ is the r^{th} derivative of its moment generating function $M(\xi) = E(e^{\xi x})$. The cumulants c_r are the coefficients in the Taylor expansion of the generating function $\ln M(\xi)$, i.e. $\ln M(\xi) = \sum_{r=0}^{\infty} c_r \xi^r / r!$. A closed form that gives the c_l's in terms of the first l moments is

$$c_l = (-1)^{l+1} \begin{vmatrix} \rho_1 & 1 & 0 & 0 & 0 & 0 & \dots & 0 \\ \rho_2 & \rho_1 & 1 & 0 & 0 & 0 & \dots & 0 \\ \rho_3 & \rho_2 & \binom{2}{1}\rho_1 & 1 & 0 & 0 & \dots & 0 \\ \rho_4 & \rho_3 & \binom{3}{1}\rho_2 & \binom{3}{2}\rho_1 & 1 & 0 & \dots & 0 \\ \rho_5 & \rho_4 & \binom{4}{1}\rho_3 & \binom{4}{2}\rho_2 & \binom{4}{3}\rho_1 & 1 & \dots & 0 \\ \vdots & \vdots & \vdots & \vdots & \vdots & \ddots & \ddots & \vdots \\ \rho_{l-1} & \rho_{l-2} & \dots & \dots & \dots & \dots & \ddots & 1 \\ \rho_l & \rho_{l-1} & \dots & \dots & \dots & \dots & \dots & \binom{l-1}{l-2}\rho_1 \end{vmatrix} . \tag{6.1}$$

When this determinant is algebraically computed, c_l is given by a sum of N_l terms of the form $d_k \rho_{s_1}^{p_1} \rho_{s_2}^{p_2} \dots \rho_{s_{n_k}}^{p_{n_k}}$, being N_l equal to the number of forms in which l can be decomposed into a sum of positive integers. These terms for $l = 1 \dots 9$ are collected in Table 6.1.

Each of them satisfies $\sum_{i=1}^{n_k} s_i \times p_i = l$. The d_k's in Table 6.1 are not directly those resulting from the expansion of determinant 6.1. They have been modified as follows in order that the c_l's satisfy the recursivity and normalization properties of cumulants: i) If the coefficient of ρ_1^l (always present) is negative we change the sign of all the d_k's. ii) We divide each d_k by the coefficient of the term ρ_1^l. iii) We divide further each d_k by the factor $l!/[\Pi_{i=1}^{k} p_i!(s_i!)^{p_i}]$. This last normalization is pertinent because each $\rho_{s_1}^{p_1} \rho_{s_2}^{p_2} \dots$ term in Table 6.1 must be replaced by its symmetrized expression. For instance, the term $\rho_1^2 \rho_2$ that appears for $l = 4$ must be replaced by $\rho_1(1)\rho_1(2)\rho_2(3,4) + \rho_1(1)\rho_1(3)\rho_2(2,4) + \rho_1(1)\rho_1(4)\rho_2(2,3) + \rho_1(2)\rho_1(3)\rho_2(1,4) + \rho_1(2)\rho_1(4)\rho_2(1,3) + \rho_1(3)\rho_1(4)\rho_2(1,2)$, so that $\rho_1^2 \rho_2$ actually has $4!/[2!1!(1!)^2(2!)^1] = 6$ components.

Table 6.1: Cumulant of orders $1 \ldots 9$. The number of terms appears in parenthesis.

$l = 1$ (1)							
ρ_1							
1							
$l = 2$ (2)							
ρ_1^2	ρ_2						
1	-1						
$l = 3$ (3)							
ρ_1^3	$\rho_1\rho_2$	ρ_3					
1	-1/2	1/2					
$l = 4$ (5)							
ρ_1^4	$\rho_1^2\rho_2$	$\rho_1\rho_3$	ρ_4	ρ_2^2			
1	-1/3	1/6	-1/6	1/6			
$l = 5$ (7)							
ρ_1^5	$\rho_1^3\rho_2$	$\rho_1^2\rho_3$	$\rho_1\rho_4$	$\rho_1\rho_2^2$	$\rho_2\rho_3$	ρ_5	
1	-1/4	1/12	-1/24	1/12	-1/24	1/24	
$l = 6$ (11)							
ρ_1^6	$\rho_1^4\rho_2$	$\rho_1^3\rho_3$	$\rho_1^2\rho_4$	$\rho_1^2\rho_2^2$	$\rho_1\rho_2\rho_3$	$\rho_1\rho_5$	ρ_3^2
1	-1/5	1/20	-1/60	1/20	-1/60	1/120	1/120
ρ_6	$\rho_2\rho_4$	ρ_2^3					
-1/120	1/120	-1/60					
$l = 7$ (15)							
ρ_1^7	$\rho_1^5\rho_2$	$\rho_1^4\rho_3$	$\rho_1^3\rho_4$	$\rho_1^3\rho_2^2$	$\rho_1^2\rho_2\rho_3$	$\rho_1^2\rho_5$	$\rho_1\rho_3^2$
1	-1/6	1/30	-1/120	1/30	-1/120	1/360	1/360
$\rho_1\rho_6$	$\rho_1\rho_2\rho_4$	$\rho_1\rho_2^3$	$\rho_3\rho_4$	$\rho_2^2\rho_3$	$\rho_2\rho_5$	ρ_7	
-1/720	1/360	-1/120	-1/720	1/360	-1/720	1/720	
$l = 8$ (22)							
ρ_1^8	$\rho_1^6\rho_2$	$\rho_1^5\rho_3$	$\rho_1^4\rho_4$	$\rho_1^4\rho_2^2$	$\rho_1^3\rho_2\rho_3$	$\rho_1^3\rho_5$	$\rho_1^2\rho_3^2$
1	-1/7	1/42	-1/210	1/42	-1/210	1/840	1/840
$\rho_1^2\rho_6$	$\rho_1^2\rho_2\rho_4$	$\rho_1^2\rho_2^3$	$\rho_1\rho_3\rho_4$	$\rho_1\rho_2^2\rho_3$	$\rho_1\rho_2\rho_5$	$\rho_1\rho_7$	$\rho_2\rho_3^2$
-1/2520	1/840	-1/210	-1/2520	1/840	-1/2520	1/5040	-1/2520
$\rho_3\rho_5$	ρ_8	$\rho_2\rho_6$	$\rho_2^2\rho_4$	ρ_4^2	ρ_2^4		
1/5040	-1/5040	1/5040	-1/2520	1/5040	1/840		
$l = 9$ (30)							
ρ_1^9	$\rho_1^7\rho_2$	$\rho_1^6\rho_3$	$\rho_1^5\rho_4$	$\rho_1^5\rho_2^2$	$\rho_1^4\rho_2\rho_3$	$\rho_1^4\rho_5$	$\rho_1^3\rho_3^2$
1	-1/8	1/56	-1/336	1/56	-1/336	1/1680	1/1680
$\rho_1^3\rho_6$	$\rho_1^3\rho_2\rho_4$	$\rho_1^3\rho_2^3$	$\rho_1^2\rho_3\rho_4$	$\rho_1^2\rho_2^2\rho_3$	$\rho_1^2\rho_2\rho_5$	$\rho_1^2\rho_7$	$\rho_1\rho_2\rho_3^2$
-1/6720	1/1680	-1/336	-1/6720	1/1680	-1/6720	1/20160	-1/6720
$\rho_1\rho_3\rho_5$	$\rho_1\rho_8$	$\rho_1\rho_2\rho_6$	$\rho_1\rho_2^2\rho_4$	$\rho_1\rho_4^2$	$\rho_1\rho_2^4$	ρ_3^3	$\rho_3\rho_6$
1/20160	-1/40320	1/20160	-1/6720	1/20160	1/1680	1/20160	-1/40320
$\rho_2\rho_3\rho_4$	$\rho_2^3\rho_3$	$\rho_4\rho_5$	$\rho_2^2\rho_5$	$\rho_2\rho_7$	ρ_9		
1/20160	-1/6720	-1/40320	1/20160	-1/40320	1/40320		

Bibliography

[1] AJ Coleman. Density matrices in the quantum theory of matter: Energy, intracules and extracules. *International Journal of Quantum Chemistry*, 1(S1):457–464, 1967.

[2] Pierre Hohenberg and Walter Kohn. Inhomogeneous electron gas. *Physical review*, 136(3B):B864, 1964.

[3] Richard FW Bader. Atoms in molecules: a quantum theory. international series of monographs on chemistry 22, 1990.

[4] Raymond Daudel, Hélène Brion, and Simone Odiot. Localizability of electrons in atoms and moleculesapplication to the study of the notion of shell and of the nature of chemical bonds. *The Journal of Chemical Physics*, 23:2080, 1955.

[5] Paul LA Popelier. Quantum chemical topology: on bonds and potentials. In *Intermolecular Forces and Clusters I*, pages 1–56. Springer, 2005.

[6] Axel D Becke and Kenneth E Edgecombe. A simple measure of electron localization in atomic and molecular systems. *The Journal of chemical physics*, 92:5397, 1990.

[7] Frank R Wagner, Miroslav Kohout, and Yuri Grin. Direct space decomposition of eli-d: interplay of charge density and pair-volume function for different bonding situations. *The Journal of Physical Chemistry A*, 112(40):9814–9828, 2008.

[8] A Martín Pendás, E Francisco, and A Costales. Perspectives for quantum chemical topology in crystallography. *Physica Scripta*, 87(4):048106, 2013.

[9] John Lennard-Jones. The molecular orbital theory of chemical valency. ii. equivalent orbitals in molecules of known symmetry. *Proceedings of the Royal Society of London. Series A. Mathematical and Physical Sciences*, 198(1052):14–26, 1949.

[10] RFW Bader and ME Stephens. Spatial localization of the electronic pair and number distributions in molecules. *Journal of the American Chemical Society*, 97(26): 7391–7399, 1975.

[11] Robert Ponec. Electron pairing and chemical bonds. chemical structure, valences and structural similarities from the analysis of the fermi holes. *Journal of Mathematical Chemistry*, 21(3):323–333, 1997.

[12] Robert Ponec. Electron pairing and chemical bonds. molecular structure from the analysis of pair densities and related quantities. *Journal of mathematical chemistry*, 23(1-2):85–103, 1998.

[13] E Francisco, A Martín Pendás, M García-Revilla, and Roberto Álvarez Boto. A hierarchy of chemical bonding indices in real space from reduced density matrices and cumulants. *Computational and Theoretical Chemistry*, 2012.

[14] Tosio Kato. On the eigenfunctions of many-particle systems in quantum mechanics. *Communications on Pure and Applied Mathematics*, 10(2):151–177, 1957.

[15] MA Blanco, A Martín Pendás, and E Francisco. Interacting quantum atoms: a correlated energy decomposition scheme based on the quantum theory of atoms in molecules. *Journal of Chemical Theory and Computation*, 1(6):1096–1109, 2005.

[16] A Martín Pendás, MA Blanco, and E Francisco. Chemical fragments in real space: definitions, properties, and energetic decompositions. *Journal of Computational Chemistry*, 28(1):161–184, 2007.

[17] E Francisco, A Martín Pendás, and MA Blanco. A molecular energy decomposition scheme for atoms in molecules. *Journal of Chemical Theory and Computation*, 2 (1):90–102, 2006.

[18] Richard FW Bader. Bond paths are not chemical bonds. *The Journal of Physical Chemistry A*, 113(38):10391–10396, 2009.

[19] Paul Ziesche. Attempts toward a pair density functional theory. *International journal of quantum chemistry*, 60:149–162, 1996.

[20] E Francisco, A Martín Pendás, and MA Blanco. A connection between domain-averaged fermi hole orbitals and electron number distribution functions in real space. *The Journal of chemical physics*, 131:124125, 2009.

[21] Paul Ziesche, Stefan Kurth, and John P Perdew. Density functionals from lda to gga. *Computational materials science*, 11(2):122–127, 1998.

[22] Mel Levy, John P. Perdew, and Viraht Sahni. Exact differential equation for the density and ionization energy of a many-particle system. *Phys. Rev. A*, 30:2745–2748, Nov 1984. doi: 10.1103/PhysRevA.30.2745. URL `http://link.aps.org/doi/10.1103/PhysRevA.30.2745`.

[23] Maria Hoffmann-Ostenhof and Thomas Hoffmann-Ostenhof. "schrödinger inequalities" and asymptotic behavior of the electron density of atoms and molecules. *Phys. Rev. A*, 16:1782–1785, Nov 1977. doi: 10.1103/PhysRevA.16.1782. URL `http://link.aps.org/doi/10.1103/PhysRevA.16.1782`.

[24] Aleš Zupan, John P Perdew, Kieron Burke, and Mauro Causa. Density-gradient analysis for density functional theory: application to atoms. *International journal of quantum chemistry*, 61(5):835–845, 1997.

[25] Richard FW Bader and H Essen. The characterization of atomic interactions. *The Journal of chemical physics*, 80:1943, 1984.

[26] Julia Contreras-García, Mónica Calatayud, Jean-Philip Piquemal, and JM Recio. Ionic interactions: Comparative topological approach. *Computational and Theoretical Chemistry*, 2012.

[27] A Martín Pendás, Aurora Costales, and Víctor Luaña. Ions in crystals: The topology of the electron density in ionic materials. i. fundamentals. *Physical Review B*, 55(7):4275, 1997.

[28] A Martín Pendás, Aurora Costales, and Víctor Luaña. Ions in crystals: the topology of the electron density in ionic materials. iii. geometry and ionic radii. *The Journal of Physical Chemistry B*, 102(36):6937–6948, 1998.

[29] John P. Perdew, Kieron Burke, and Matthias Ernzerhof. Generalized gradient approximation made simple. *Phys. Rev. Lett.*, 77: 3865–3868, Oct 1996. doi: 10.1103/PhysRevLett.77.3865. URL `http://link.aps.org/doi/10.1103/PhysRevLett.77.3865`.

[30] Stefan Grimme. Semiempirical gga-type density functional constructed with a long-range dispersion correction. *Journal of computational chemistry*, 27(15):1787–1799, 2006.

[31] G Kresse and J Furthmüller. Software vasp, vienna (1999). *Phys. Rev. B*, 54(11): 169, 1996.

[32] Julia Contreras-García, Erin R Johnson, Shahar Keinan, Robin Chaudret, Jean-Philip Piquemal, David N Beratan, and Weitao Yang. Nciplot: a program for plotting noncovalent interaction regions. *Journal of chemical theory and computation*, 7(3):625–632, 2011.

[33] Alberto Otero-de-la Roza, Erin R Johnson, and Julia Contreras-García. Revealing non-covalent interactions in solids: Nci plots revisited. *Physical Chemistry Chemical Physics*, 14(35):12165–12172, 2012.

[34] Sason Shaik, David Danovich, Bernard Silvi, David L Lauvergnat, and Philippe C Hiberty. Charge-shift bondinga class of electron-pair bonds that emerges from valence bond theory and is supported by the electron localization function approach. *Chemistry-A European Journal*, 11(21):6358–6371, 2005.

[35] Julia Contreras-García, Weitao Yang, and Erin R Johnson. Analysis of hydrogen-bond interaction potentials from the electron density: Integration of noncovalent interaction regions. *The Journal of Physical Chemistry A*, 115(45):12983–12990, 2011.

[36] A Martín Pendás, Miguel A Blanco, Aurora Costales, Paula Mori Sánchez, and Víctor Luaña. Non-nuclear maxima of the electron density. *Physical review letters*, 83(10):1930–1933, 1999.

[37] Víctor Luaña, Paula Mori-Sánchez, Aurora Costales, MA Blanco, and A Martín Pendás. Non-nuclear maxima of the electron density on alkaline metals. *The Journal of chemical physics*, 119:6341, 2003.

[38] Sason Shaik, David Danovich, Wei Wu, and Philippe C Hiberty. Charge-shift bonding and its manifestations in chemistry. *Nature chemistry*, 1(6):443–449, 2009.